Highlights

- Stratigraphical and sedimentological revision of Upper Triassic strata from Aghdarband Basin with new remarks on the evolution of the basin
- Palynological analyses support an assignment of the basal Miankuhi Formation to the latest early to late Carnian age corresponding to the Carnian Pluvial Episode (CPE)
- New quantitative palynological data suggest a more humid climate in the lower part of the Miankuhi Formation, supporting a strong correlation with the Carnian Pluvial Episode
- The significant unconformity at the base of the Miankuhi Formation was formed as a result of a drop in sea level caused by a climate change towards humidity
- The data provide the best available estimate for the onset of Eo-Cimmerian orogeny older than Middle Norian (217 ± 1.7 Ma) but younger than the late Carnian, at least in the case of the NE Iranian segment of the Paleotethys suture zone

Disentangling climate signal from tectonic forcing: the Triassic Aghdarband Basin (Turan domain, Iran)

Mina Mazaheri-Johari[1*], Guido Roghi[2], Marcello Caggiati[1], Evelyn Kustatscher[3,4], Ebrahim Ghasemi-Nejad[5], Andrea Zanchi[6], Piero Gianolla[1]

[1]Department of Physics and Earth Sciences, University of Ferrara, Via Saragat 1, Block B, Ferrara 44100, Italy. E-mail: mzhmni@unife.it, marcello.caggiati@unife.it, glr@unife.it

[2] Institute of Geosciences and Earth Resources - CNR, Via Gradenigo 6, Padova 35131, Italy. E-mail: guido.roghi@igg.cnr.it

[3]Department of Earth and Environmental Sciences, Paleontology & Geobiology, Ludwig-Maximilians-Universität München, Richard-Wagner-Straße 10, 80333 München, Germany. E-mail: Evelyn.Kustatscher@naturmuseum.it

[4]SNSB-Bayerische Staatssammlung für Paläontologie und Geologie, Richard-Wagner-Straße 10, 80333 München, Germany. E-Mail: Evelyn.Kustatscher@naturmuseum.it

[5]Department of Geology, Faculty of Science, University of Tehran, Enghelab Square, Tehran 1417935840, Iran. E-mail: eghaseminejad@gmail.com

[6]Department of Earth and Environmental Sciences, University of Milano-Bicocca, Piazza della Scienza 1, 20126 Milan, Italy. Email: andrea.zanchi@unimib.it

Abstract

The Middle-Upper Triassic Aghdarband Basin, NE Iran, consists of a strongly deformed marine and non-marine stratigraphic succession, deposited along the southern margin of Asia in a highly complex tectonic context related to a back-arc setting. The youngest deformed units of the Aghdarband area consist of a rather monotonous sequence of brown-colored shales, with intercalations of siltstones and fine-grained sandstones forming the Miankuhi Formation. The shale-dominated Miankuhi Formation rests on an unconformity surface, separating it from the underlying Sina Formation. A multidisciplinary study based on sedimentological, palynological, and paleobotanical data permits to reconstruct the depositional environments, sedimentary evolution, and paleoclimate conditions of the upper Sina and the lowermost Miankuhi formations. The palynological association of the lowermost part of the Miankuhi Formation yielded sporomorphs of the latest early Carnian to early late Carnian age. Qualitative and quantitative analyses document a shift from xerophytic associations in the upper Ladinian (upper Sina Formation) to hygrophytic assemblages in the Carnian (lower Miankuhi Formation). This increase in hygrophytic elements is also observed in coeval Tethyan outcrops at the same latitudinal belt, suggests a more humid climate in the lower part of the Miankuhi

Formation, and correlates this part of the succession with a record of the Carnian Pluvial Episode. The sedimentological and stratigraphical analyses show an evolution from prodelta to delta setting in the Upper Sina Formation, then an unconformity enhanced by an interval of fluvial deposits with histosol levels in the basal Miankuhi Formation, in correspondence with the hygrophytic assemblages. The unconformable boundary between the Miankuhi and the Sina formations is, consequently, interpreted as a result of the sea-level fall associated with the humid climate shift, occurring in close association with the first effects of the Eo-Cimmerian orogeny along the suture zone, taking to a regional reorganization of the basins architecture and the end of volcanic activity in the back-arc region. The main deformations related to the Eo-Cimmerian event thus, correspond in the Aghdarband Basin to the tectonic event that deformed the Miankuhi Formation. This event is probably older than the middle Norian (217.1 ± 1.7 Ma) but younger than the late Carnian, testifying to a diachronicity in the record of collision along the Iranian Cimmerian blocks and Southern Laurasia according to the different considered structural positions.

Keywords: Miankuhi Formation; Cimmerian Orogeny; Carnian Pluvial Episode; Palynology; Kopeh-Dagh; Triassic

1. Introduction

During the Late Triassic to Early Jurassic Cimmerian Orogeny, the Iran plate collided with the southern margin of Laurasia (Turan domain) and formed a single sedimentary province. There is still considerable controversy regarding the timing and dynamics of this orogenetic process, but it had a profound effect on the Late Triassic and Jurassic sedimentation patterns, giving origin to a series of unconformities (e.g., Stöcklin, 1974; Boulin, 1988; Ruttner, 1991; Saidi et al., 2015; Alavi et al., 1997; Stampfli and Borel, 2002; Horton et al., 2008; Fürsich et al., 2009a; Wilmsen et al., 2009 a,b; Zanchi et al., 2009 a, b; Zanchetta et al., 2013; Zanchi et al., 2016; Seyed-Emami et al., 2021). The effect of this orogeny is registered in the Aghdarband Basin, which is located in the southern part of the Kopeh-Dagh Range on the southern margin of Laurasia (NE Iran) and consists mainly of Triassic successions (Ruttner, 1991; Alavi et al., 1997; Zanchi et al., 2009a, 2016; Sheikholeslami and Kouhpeyma, 2012; Zanchetta et al., 2013). The Middle-Upper Triassic succession of the Aghdarband Basin consists of the deep-water to prodelta-delta volcanoclastic sequences of the Sina Formation (Ruttner, 1991; Mazaheri-Johari et al., 2021) and the shale-dominated Miankuhi Formation (Ruttner, 1991).

The two formations are separated by an unconformable boundary corresponding to the end of the deposition of marine arc-related volcaniclastics in the area (Sina Formation), and according to Ruttner (1991) and Zanchi et al. (2016), it records the onset of the Eo-Cimmerian collision. The Cimmerian compressional event produced wide deformations in the Triassic units of the area, and the Miankuhi Formation is the youngest unit subjected to this deformative event (Alavi, 1991; Alavi et al., 1997; Sheikholeslami and Kouhpeyma, 2012; Zanchetta et al., 2013; Zanchi et al., 2016). Besides the complex tectonic history of the Triassic succession, not much is known about the age of the Miankuhi Formation, except few studies on plant megafossils and marine palynology (dinoflagellate cysts) of its lowermost part suggesting a pre-Rhaetian age (Boersma and Van Konijnenburg-van Cittert, 1991; Ghasemi-Nejad et al., 2008). The macroplant assemblage (sphenophytes, ginkgophytes, conifers, and *incertae sedis*), palynological associations (Mazaheri-Johari et al., 2021), and stratigraphical observations in the basal Miankuhi Formation reconstruct these strata as continental to marginal marine deposits formed under humid environmental conditions during the early-late Carnian.

The following three hypotheses can be proposed for the origin of the unconformity and the coal-bearing sediments at the base of the continental deposits of the Miankuhi Formation: (1) The slight expressed unconformity represents the oldest effects of the Eo-Cimmerian collision, followed by a subsequent strong deformation affecting the whole Triassic succession related to the progressive propagation of the deformation front across the arc region within the upper plate (Zanchi et al., 2016). This may have caused a vertical uplift of the Kopeh-Dagh basement resulting in erosion and accumulation of continental sediments due to the balance between active tectonic regimes and surface processes; (2) The northward movement of Laurasia and the latitudinal shift towards a more humid belt resulted in a zonal climate control on the sedimentary facies, increasing noticeably the sedimentation and precipitation along the whole southern margin of Laurasia; (3) A local record of the so-called Carnian Pluvial Episode (CPE), a global climatic disturbance with a short duration (Simms and Ruffell, 1989; Ruffell et al., 2016; Miller et al., 2017; Dal Corso et al., 2018, 2020; Colombi et al., 2021), influenced the marginal marine to continental setting increasing the runoff, sudden input of immature siliciclastics, stream rejuvenation and fluvial incision, development of paleosols typical of humid climates (Breda et al., 2009; Kozur and Bachmann, 2010), and a marked sea-level fall (Roghi et al., 2010; Stefani et al., 2010; Arche and López-Gómez, 2014; Gattolin et al., 2015; Shi et al., 2017; Barrenechea et al., 2018; Klausen et al., 2020).

In this paper, we propose an interdisciplinary study of three stratigraphic successions from the Upper Triassic tectonic unit 2 of the Aghdarband Basin (Ruttner, 1991; Zanchi et al., 2016).

Stratigraphic, sedimentological, and qualitative and quantitative palynological analyses were carried out for a biostratigraphic characterization, as well as paleoclimatic and paleoenvironmental reconstructions in order to test the above-mentioned hypotheses.

2. Geological setting

The Aghdarband Basin occupies the southern part of the Kopeh-Dagh Range in Northeast Iran (Fig. 1). During the Late Triassic, it was part of the southern margin of Laurasia, positioned at ~35–45º N (Mattei et al., 2014; Muttoni et al., 2015; Matthews et al., 2016; Cao et al., 2017; Barrier et al., 2018) (Fig. 2). The sedimentation pattern of the studied area is mostly governed by Triassic carbonate-siliciclastic sediments (Fig. 3), which are intensely deformed due to the Cimmerian Orogeny. During this important orogenic event affecting the southern Eurasian margin (Turan domain), the Iran plate as part of the Cimmerian blocks detached from Gondwana at the end of the Paleozoic and collided with the southern margin of Laurasia during the Late Triassic due to the closure of the Paleotethys (e.g., Stöcklin, 1974; Sengör, 1979, 1984, 1990; Gaetani, 1997; Besse et al., 1998; Stampfli and Borel, 2002; Wilmsen et al., 2009a; Zanchi et al., 2009b; Muttoni et al., 2009; Robinson et al., 2012; Sheikholeslami and Kouhpeyma, 2012; Mirnejad et al., 2013; Barrier et al., 2018). The northward subduction of the Paleotethys below the southern margin of Laurasia (Turan domain) resulted in the formation of an arc setting with Triassic deposits (Ruttner, 1991; Balini et al., 2009, 2019; Sheikholeslami and Kouhpeyma, 2012) in the Aghdarband Basin (Ruttner, 1991; Alavi et al., 1997) (Fig. 2). This basin is structurally divided into three tectonic units (Ruttner, 1991; Zanchi et al., 2016): (1) the Southern unit consisting of coarse-grained conglomerates, sandstones, and slates of ?latest Permian to earliest Triassic age (Ruttner, 1991; Alavi et al., 1997; Zanchi et al., 2016); (2) the Northern unit as part of the Eurasian arc-related Turan domain (Ruttner, 1991; Natal'in and Şengör, 2005; Zanchi et al., 2016) consisting of upper Paleozoic rocks; (3) a central part comprising mostly marine fossiliferous Triassic successions (Ruttner, 1991; Zanchi et al., 2016; Balini et al., 2019). The central part is further subdivided into three tectonic subunits named units 1, 2, and 3 (Fig. 1) from North to South (Ruttner, 1991; Zanchi et al., 2016). Most of the sedimentary successions are strongly deformed in all tectonic units. The deformation style of sediments in unit 1 is represented by folding and faulting controlled by a transpressional tectonic regime, whereas thrusting is the dominating deformation style of the successions deposited in units 2 and 3 (Ruttner, 1991; Zanchi et al., 2016). From the early '70s, several studies were conducted on the central and eastern parts of the Aghdarband Basin by different research groups. The comprehensive studies performed in 1991 by Anton Ruttner are among the most important ones, including a detailed geological map at 1:12,500 scale (Ruttner, 1991: pl. 1).

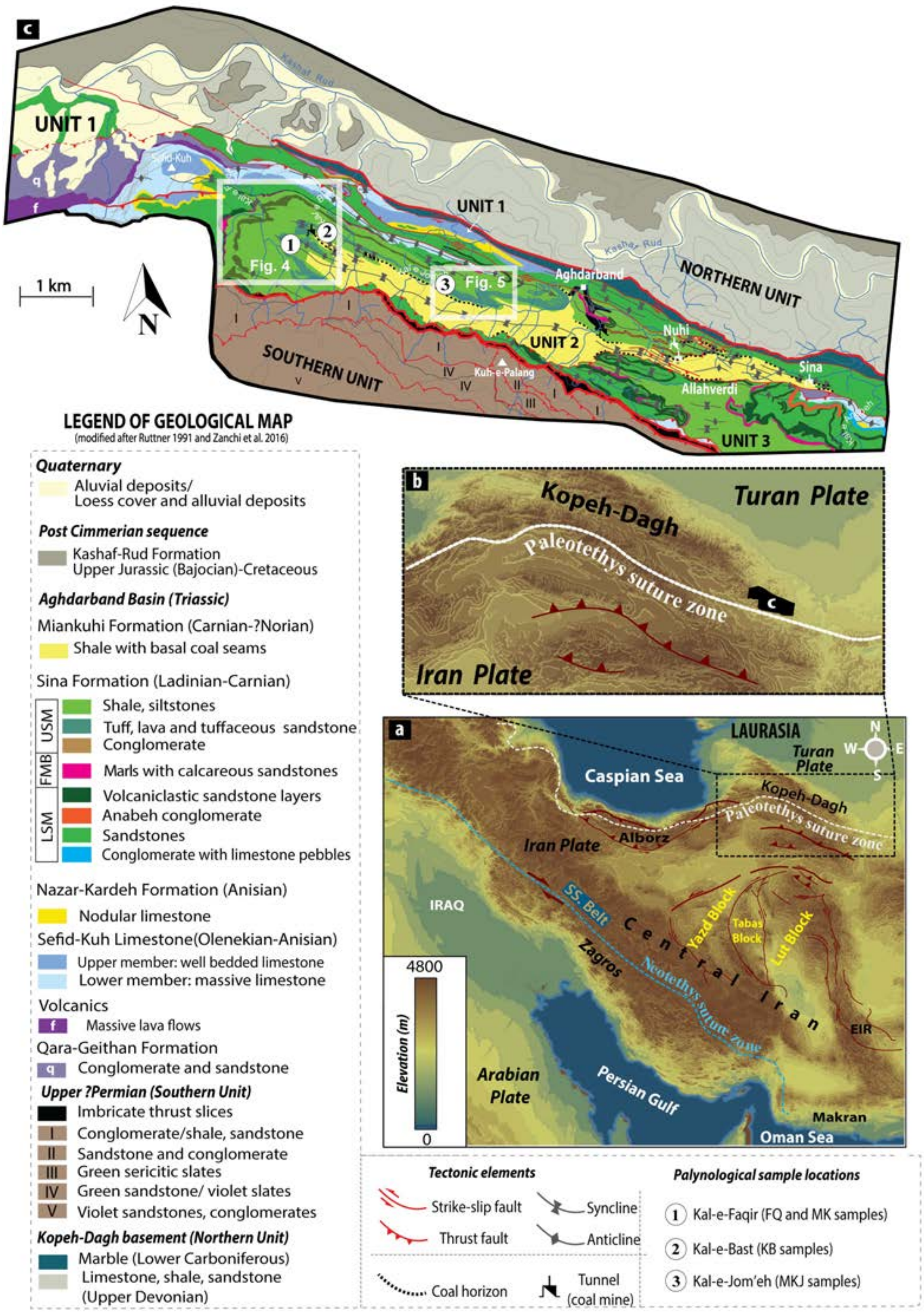

Fig. 1. (a) Main structural zones of the area (after Stocklin and Nabavi, 1973; Berberian and King, 1981; Allen et al., 2004, 2011; Morley et al., 2009; Nozaem et al., 2013; Calzolari et al., 2016). (**b**) Detail of the Kopeh-Dagh Range and the location of the studied area (Aghdarband Basin). (**c**) Geological map of the Aghdarband area showing the three tectonic units and the various formations of the Aghdarband Basin (modified after Ruttner, 1991 and Zanchi et al., 2016), and locations of the studied sections (1: Kal-e-Faqir composite section, 2: Kal-e-

Bast section, 3: Kal-e-Jom'eh section). Abbreviations: SS. Belt: Sanandaj-Sirjan Belt; EIR: East Iranian Range; LSM: Lower Sandstone Member; FMB: Faqir Marl Bed; USM: Upper Shale Member.

3. Materials and methods

Three stratigraphic sections have been studied in the tectonic unit 2 of the central part of the Aghdarband Basin, respectively the Kal-e-Faqir, the Kal-e-Bast, and the Kal-e-Jom'eh sections (Fig. 1, 4-5). A multidisciplinary approach involving stratigraphy, sedimentology, and palynology has been adopted to provide a better understanding of the sedimentary geology, biostratigraphy, and paleoclimatology of the studied successions. High-definition field-image processing enhances the sedimentological observations and helps to define geometric relationships between different stratigraphic units. This method, combined with detailed stratigraphic and sedimentological analyses, permitted us to review the geological map (Figs. 4, 5) of the surroundings of each section, based on the original map by Ruttner (1991).

Forty-three samples were collected for qualitative and quantitative palynological analysis, about 50% were productive, yielding sporomorphs. Rock samples were crushed and treated with HCl (37%) and HF (47%) to dissolve the non-organic material. After washing and sieving (15 μm nylon mesh), the residue was stored in water and then strew mounted onto microscope slides using Entellan glue as the mounting medium. The quantitative analysis was performed by consecutively counting a relative number of grains per sample (Visscher and van der Zwan, 1981), depending on the preservation of the organic residues in order to detect changes in the vegetation composition along the studied sections. The vegetational interpretations were carried out based on the terrestrial sporomorphs' divisions into the major plant groups sphenophytes, horsetails, ferns, cycadophytes/ginkgophytes, seed ferns, and conifers. Relative abundances were organized from most xerophytic to most hygrophytic elements inspired by Visscher and Van der Zwan (1981) and Visscher et al. (1994). The microscope slides were studied under a Leica DM750 light microscope, and the index species were photographed using a Leica ICC50 W digital camera (Plates I-III). The slides are housed in the Department of Physics and Earth Sciences of the University of Ferrara.

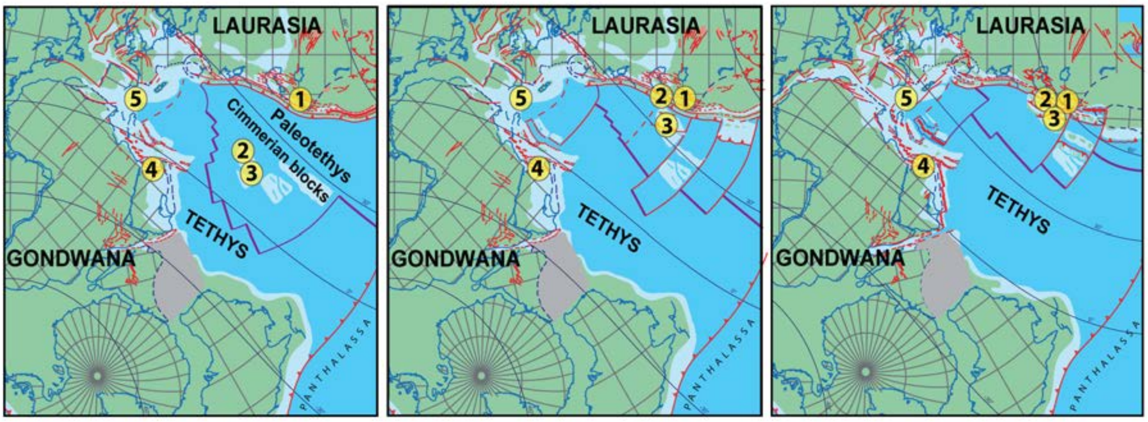

Fig. 2. Late Triassic paleogeographic position of the studied area (1 = Aghdarband area, 2 = Alborz, 3 = Central Iran, 4 = North Iraq, 5 = Southern Alps) (modified after Barrier et al., 2018).

4. Stratigraphy

Triassic successions in Iran are exposed in Central Iran (Tabas, Nayband, Kerman, Zofreh-Soh, Abadeh), North Iran (Alborz), Zagros, and in the tectonic window of Aghdarband in northeastern Iran (Berberian and King, 1981; Ruttner, 1991; Alavi et al., 1997; Buryakovsky et al., 2001; Robert et al., 2014). The Triassic rocks of the Aghdarband Basin are characterized by marine and non-marine sediments forming the Aghdarband Group. The Aghdarband Group has been divided into four formations based on their lithological and paleontological content (Ruttner, 1991) (Fig. 3). The lowermost formation of the Aghdarband Group is the Olenekian to middle Anisian Sefid-Kuh Limestone (Sdkh. Lst. in Fig. 3) (Ruttner, 1991; Balini et al., 2019; Liaghat et al., 2021) overlying the ?late Permian–Early Triassic volcanoclastic conglomerates of the Qara-Qeitan Formation (Ruttner, 1991; Eftekharnezhad and Behroozi, 1991; Alavi et al., 1997; Balini et al., 2009; Zanchi et al., 2016). The former unit is generally overlain by the relatively deep-water fossiliferous cherty limestones of the Nazar-Kardeh Formation (Nzkd. in Fig. 3), Bithynian in age (Krystyn and Tatzreiter, 1991; Balini et al., 2019). The Sefid-Kuh and Nazar-Kardeh formations were deformed and eroded, and subsequently, a tectonically controlled basin was formed. This basin was then filled by a marine, volcanoclastic succession called Sina Formation (Ruttner, 1991; Baud et al., 1991b; Balini et al., 2019). Moving upwards, the shale-dominated Miankuhi Formation (Mnkh. in Fig. 3) rests on the Sina Formation, divided by an unconformity surface.

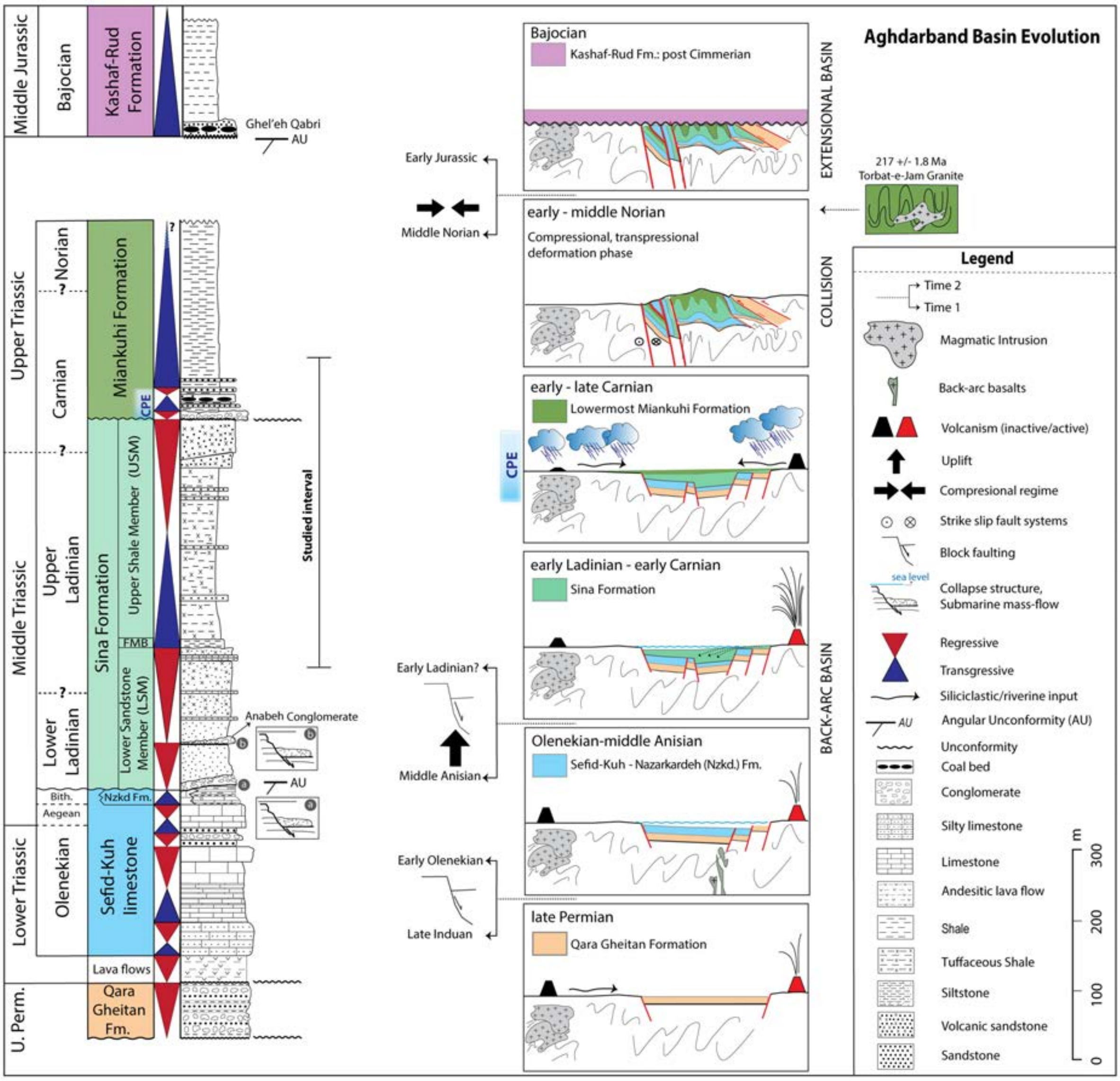

Fig. 3. General lithostratigraphic column of the Triassic sequence of the Aghdarband Basin (modified from Ruttner, 1991, 1993; Zanchi et al., 2016; Balini et al., 2019) and basin evolution (modified after Zanchi et al., 2016). Abbreviations: u. Perm.: upper Permian; Bith: Bithynian; Nzkd Fm.: Nazar-Kardeh Formation; FMB: Faqir Marl Bed.

4.1. The Sina Formation

The Sina Formation has been investigated in detail in the upper part of the Kal-e-Faqir composite section. This section is the most complete one, covering both the Sina and the Miankuhi formations, and is composed of five segments (Fig. 4). In some localities, there are lines of monogenic conglomerates along the angular unconformity at the base of the Sina Formation (Ruttner, 1991; Balini et al., 2019). The lower part of the Sina Formation, named *Lower Sandstone Member* (LSM), is characterized by the prevalence of dark-green, decimeterthick beds of coarse to medium-grained volcanoclastic sandstones, brownish on the weathered surface, with dark (green to violet) tuffaceous shale intercalations (in some places up to one meter thick). Sandstones commonly show normal grading and other turbiditic features and are organized in (decameter) thick stacks of beds alternating with minor intervals where greenish to dark greyish pelites prevail. Tuffaceous limestones have also been found. A decameter layer composed of polygenic conglomerate beds and intercalated coarse-grained sandstone crops out in the eastern part of the Aghdarband Basin (Anabeh Conglomerate Bed, unit 3, Ruttner, 1991; Balini et al., 2019), within the lower LSM. The upper part of the LSM is characterized by a coarsening and thickening upward sequence mainly composed of thick-bedded litharenites and calcareous tuffaceous sandstones, producing an easily identifiable cliff. In this part, well-preserved ammonoid remnants have been found. The sharp reappearing of fine muds above the LSM marks a well-visible ledge (Fig. 6a). It identifies the transition to the *Faqir Marl Bed* (FMB), composed of greenish calcareous pelites, pink marls, tuffaceous crinoidal packstone, and rare tuffaceous calcareous sandstone intercalations. Beyond small local changes in thickness, the FMB represents an important marker interval in the succession. In addition to crinoids, cephalopods, brachiopods, and pelagic bivalves are common (Kristan-Tollmann et al., 1991; Krystyn and Tatzreiter, 1991; Siblik, 1991). The unit extends upward for about 25 meters, even if its middle to the upper part is often not exposed because of debris cover.

Above the FMB, a very thick siliciclastic succession occurs, named *Upper Shale Member* (USM). Its lower part is commonly composed of greenish shales and siltites, and less common thin-bedded, poorly cemented, dark green to brown tuffaceous sandstone intercalations. About 45 meters upward in the Kal-e-Faqir composite section, a 10 meters thick, tuffaceous litharenite-rich interval occurs, with plant fragments, flow casts, and other unidirectional tractive current indicators (Ruttner, 1991), in turn, followed by pelites with thin sandstone intercalations. Compared to the LSM, an increase in the content of metamorphic and plutonic grains from the crystalline basement has been described (Ruttner, 1991; Baud et al., 1991a). At about 120 m from the base, the member shows a fining and thinning upward trend, with sandstone intercalations becoming increasingly rare (Fig. 6b). On the other hand, thin mudstone to wackestone layers occur intercalated in fine siliciclastics. Several pelagic crinoids (Fig. 6c) have been found in this interval, together with brachiopods and pelagic bivalves. Toward the top of the USM, the stacking pattern changes to thickening and coarsening upward, culminating in dm-thick sandstone layers with silty intercalations and the transition to the *Upper Litharenite lithofacies (ULL)* (Fig. 6d). The transition is gradual, occurring both upward and laterally (Fig. 6e). The ULL comprises decameter sets of massive to clinostratified litharenites, commonly with an erosive base, separated by thin intervals where silty intercalations are common. Toward the top of the sandstone unit, erosive channels and accretionary forms have been locally identified. Wood and plant debris are also common in some layers. A lateral transition toward dark shaly pelites occurs.

4.2. The Miankuhi Formation

Polygenic conglomerate beds with a sharp erosive base on the USM mark the unconformity at the base of the Miankuhi Formation. In the Kal-e-Faqir composite section (Fig. 4), the conglomerate is followed upwards by a succession of brownish to yellowish pelites with thin, tabular to lenticular sandstone intercalations. Less frequently, siltstones and sandstones (sometimes tuffaceous) show small- and large-scale cross-bedding and are organized in sets forming overall lenticular bodies. These patterns become very common after about 30 m upward in the section (Fig. 7a, b), where channel sandstone bodies in part crosscut themselves, sometimes resulting in amalgamated banks. Polygenic conglomerates at the base of cross-bedded sandstones are also frequent. At 55 m from the base of the formation, the occurrence of medium-large sized channels decreases, and sandstone bodies are limited to lenticular or tabular thin layers intercalated with brownish pelites yielding a marine benthonic microfauna typical for a stressful environment (Oberhauser and Prey in Ruttner, 1991). A similar succession marking the base of the Miankuhi Formation has also been reported in the area south of the Kal-e-Bast creek (Ruttner, 1991), where layers of 2-3 meters thick polygenic conglomerates and cross-bedded coarse sandstones irregularly cut the top of the Sina Formation (i.e., the top litharenite unit) and underneath a one-meter-thick coal seam (Fig. 7c). The Minankuhi Formation is also present near the Kal-e-Faqir composite section and can be correlated to its upper part, whereas in the Kal-e-Jom'eh section, it occurs together with coaly shales and shales with diagenetic nodules and common plant root traces, intercalated with sandstones (Fig. 7d). In this continental interval, histosol levels with marls full of plant debris and thin coal layers have also been observed.

Above the coal seam, yellowish sandstones and sandy shales occur again for less than 10 meters and shift upwards to shale and thin sandstone alternations. The Miankuhi Formation continues for about 150 m with a monotonous succession of shales, apparently without any important change in the depositional style. The Miankuhi Formation, differently to the other formations of the Aghdarband tectonic window, is not confined to the Aghdarband basin but is present in a large area of Tarik Dareh region (Kopeh-Dagh), extending from Aghdarband to Torbat Jam with a thickness of about 500 meters (Aghanabati, 2004; Torshizian, 2016). North of Torbat Jam, coal-bearing facies of the unit is intruded by the Torbat Jam Granite with an U-Pd zircon radiometric age of 217 ± 1.7 Ma (Zanchetta et al., 2013), which is in turn non conformably covered by the basal facies of the Jurassic Kashaf Rud Formation. Outside the studied area, this formation is unconformably covered by basal sandstones of the Ghal’eh Qabri Shales. The latter were dated to the Rhaetian by Ruttner (1991, 1993) and Boersma and Van Konjnenburg-van Cittert (1991) but were recently assigned to the basal Kashaf-Rud Formation of Bajocian age, dated by ammonoids (Seyed-Emami, 2003; Taheri et al., 2009; Seyed-Emami et al., 2021).

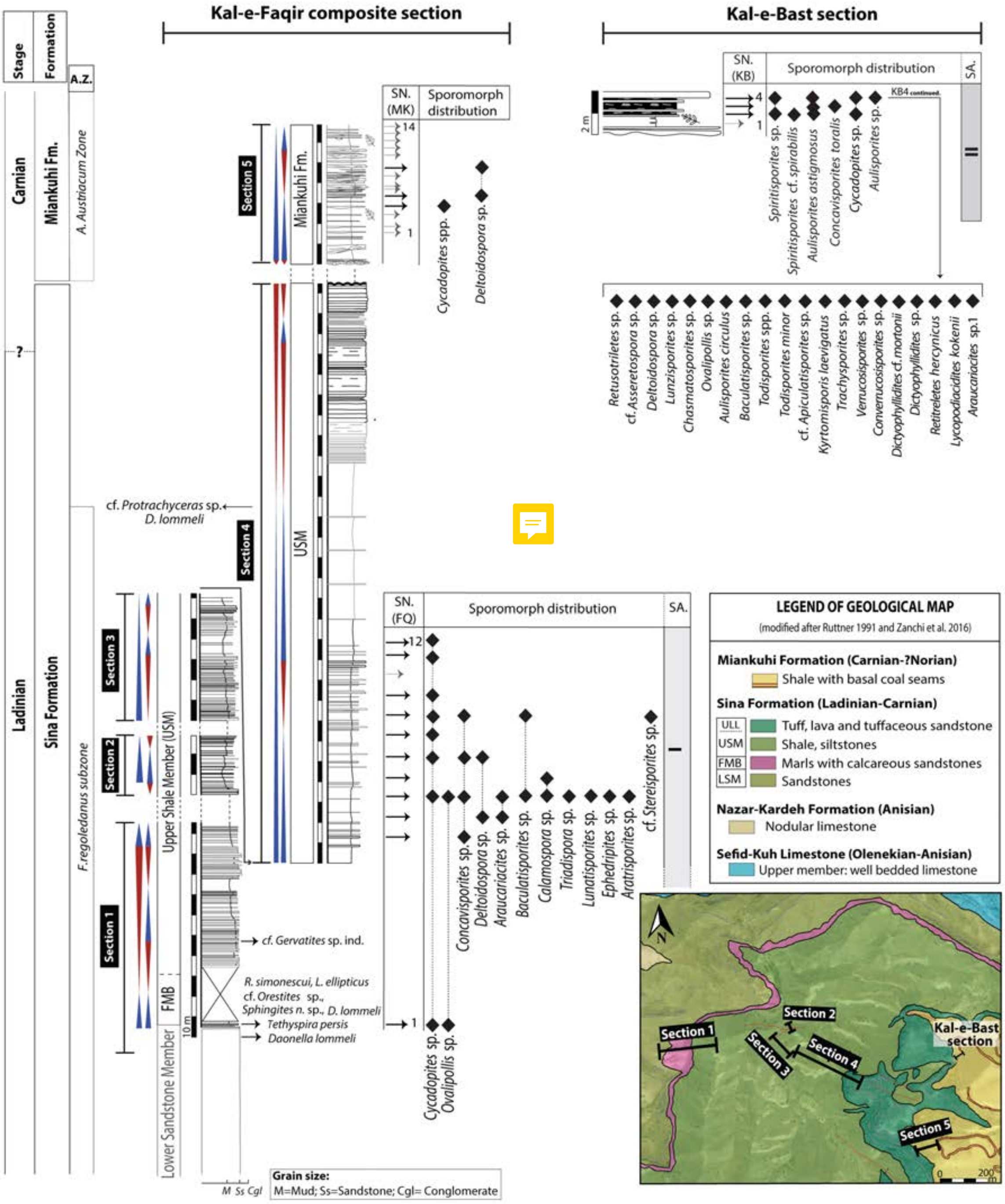

Fig. 4. Lithostratigraphy of the Triassic (upper Ladinian-Carnian) uppermost Sina and lowermost Miankuhi formations from the Kal-e-Faqir composite section and the Kal-e-Bast section, Aghdarband, with the transgressive/regressive trends, re-drawn geological map of the area surrounding the studied sections, and distribution of sporomorph assemblages. Ammonoids and Bivalvs from Krystyn and Tatzreiter (1991) and Balini et al. (2019). Black arrows indicate the palynological-productive samples. Abbreviations: SA. Sporomorph assemblage; SN: Sample number; A.Z.: Ammonoid Zone; *R. simonescui*: *Romanites simonescui*; *L. ellipticus*: *Lobites ellipticus*; *D. lommeli*: *Daonella lommeli*; *A. austriacum*: *Austrotrachycera austriacum*; FMB: Faqir Marl Bed.

5. Biostratigraphy

Conodont samples with *Gondolella costricta* and *Gondolella mombergensis* have been reported by Ruttner (1991) for the lower part of the LSM. The conodont fauna assigns the lowermost part of the succession to an early Ladinian age (*Curionii* Zone; Balini et al., 2010). *Traumatocrinus caudex*, reported by Ruttner (1991) from the middle part of the LSM (tens of meters above the Anabeh Conglomerate Bed), is a crinoid species present in the upper Ladinian to lower Julian of the Southern Alps, Northern Calcareous Alps, and China (Bittner, 1895; Wohrmann, 1889; Kristan-Tollmann et al., 1991; Hagdorn et al., 2007). The occurrence of *Monophyllites* sp. and *Daonella lommeli* (Ruttner, 1991; Krystyn and Tatzreiter, 1991) is consistent with a late Ladinian age for the upper part of the LSM. Frequent findings of some peculiar fossil species in the FMB, such as *Romanites simonescui* among ammonoids and the brachiopod *Tethyspira persis* (Ruttner, 1991 and ref. therein) allow dating the entire FMB to the uppermost Ladinian (*Frankites regoledanus* ammonoid subzone: Krystyn and Tatzreiter, 1991; Balini et al., 2019). Almost all the USM can be referred to the same substage because of the occurrence of *D. lommeli* and *Protrachyceras* spp. in the upper part of the member, just below the boundary with the ULL. The latter is lacking useful biostratigraphic markers but has been assigned by Ruttner (1991) to the early Carnian, due to the presence of an upper Triassic radiolarian and sponge association in the uppermost Sina Formation. (Donofrio, 1991).

The benthic foraminifera identified a restricted environment, whereas a macrofossil plant assemblage and poorly preserved aquatic palynomorphs (dinoflagellates) suggest a Norian (Boersma and Van Konijnenburg-van Cittert, 1991; Ghasemi-Nejad et al., 2008) and preliminary palynological analyses a Carnian age (e.g., Mazaheri-Johari et al., 2021) for the lowermost Miankuhi Formation.; more details on palynological data will be given below:

6. Palynology

All palynological assemblages are dominated by spores and pollen grains, whereas marine elements are rare. Amorphous organic matter (AOM) is rare and present in few slides only. Dark brown, mostly angular wood particles with subordinate angular black particles are also present. The palynological assemblages vary noticeably in preservation but in general, they are not well-preserved, precluding sometimes precise species identification. Although many forms have been classified only at the genus level, some important key species have been identified. A total of 30 terrestrial sporomorph taxa and several types of aquatic palynomorphs are detected, including freshwater algae.

6.1. Palynological composition of the sections

6.1.1. Kal-e-Faqir composite section

The studied sequence in the Kal-e-Faqir valley, west of Miankuhi (36.00°N, 60.80°E; Fig. 4) covers both the Sina and the Miankuhi formations and consists dominantly of greenish shales and siltites with thin-bedded limestone and fine to coarse-grained sandstone intercalations. Twelve samples from the USM of the Sina Formation, Faqir (FQ) samples, were collected at regular intervals (sampling step is 10 meters) for palynological investigations. The samples yielded relatively well-preserved assemblages dominated by terrestrial sporomorphs belonging to the sphenophytes (*Calamospora* sp.), ferns (*Deltoidospora* sp., *Concavisporites* sp., *Baculatisporites* sp.), cycads/ginkgophytes (*Cycadopites* sp.), seed ferns, and conifers (*Ovalipollis* sp., *Triadispora* sp., *Lunatisporites* sp., *Araucariacites* sp.) (Fig. 4). In the upper part of the Kal-e-Faqir composite section (lowermost Miankuhi Formation), 14 samples were collected (MK samples) at regular intervals (sampling step varying from 2 to 6 meters), yielding spores represented by *Deltoidospora* sp. and gymnosperm pollen grains of the *Cycadopites* type (Fig. 4).

6.1.2. Kal-e-Bast section

The studied sequence lies in the Kal-e-Bast valley, west of Miankuhi (36.00°N, 60.81°E; Fig. 4) and consists of the lowermost Miankuhi Formation characterized by microconglomerate with shale intercalations, plant-bearing coaly shales, greenish clays with plant roots, coal beds, and sandstone layers. Palynological samples collected from the coal levels (KB samples) yielded a very rich spore assemblage consisting of *Deltoidospora* sp., *Concavisporites toralis*, *Todisporites minor*, *Todisporites* spp., *Verrucosisporites* sp., *Converrucosisporites* sp., *Trachysporites* sp., *Dictyophyllidites* cf. *mortonii, Dictyophyllidites* sp*., Retitriletes hercynicus*, cf. *Apiculatisporites* sp., *Lycopodiacidites kokenii, Lunzisporites* sp., *Baculatisporites* sp., cf. *Asseretospora* sp., and *Kyrtomisporis laevigatus* along with the pollen species *Spiritisporites* cf. *spirabilis*, *Spiritisporites* sp., *Aulisporites astigmosus*, and *Aulisporites circulus* (Fig. 4). To the gymnosperms belong also *Araucariacites* sp. 1 and *Cycadopites* sp.

6.1.3. Kal-e-Jom'eh section

This section in the Kal-e-Jom'eh Valley (35.99°N, 60.84°E; Fig. 5) consists of the lower part of the Miankuhi Formation characterized by conglomerate with small pebbles, sandstone, shaly sandstone, shale, and coaly shale beds. The Miankuhi Formation in the Kal-e-Jom'eh section was analyzed with a sampling step varying from 50 cm to 2.5 meters. A total of 13 samples (MKJ samples) were collected and investigated. Most samples are characterized by relatively rich terrestrial and rare marine components. Marine elements (*Micrystridium* sp.) come from the lower part of the measured section, whereas the remaining part of the section is dominated by terrestrial palynomorphs, including the bennettitalean pollen *Aulisporites* (*A. astigmosus* and *A. circulus*), *Cycadopites* spp., *Spiritisporites* sp., and *Todisporites minor*. In the upper part of the succession (sample MKJ 13) were also identified *Equisetosporites* sp. and *Annulispora* sp. (Fig. 5).

6.2. Palynostratigraphic assemblages

Almost 23 pollen samples were productive both from the Sina and Miankuhi formations. Based on the stratigraphic distribution of the various species, two main pollen assemblage are distinguished for the upper Sina Formation (Shale Member) and the lowermost part of the Miankuhi Formation (Fig. 4 and 5):

Assemblage I is defined by the presence of *Deltoidospora* sp., *Concavisporites* sp., *Baculatisporites* sp., *Calamospora* sp., *Cycadopites* sp., *Triadispora* sp., *Lunatisporites* sp., and *Araucariacites* sp. It is typical for the upper Sina Formation (Shale Member) of the Kal-e-Faqir composite section. The assemblage is, thus, composed of cycadophyte (*Cycadopites* sp.) and conifer (*Triadispora* sp., *Lunatisporites* sp., *Araucariacites* sp.) pollen grains as well as

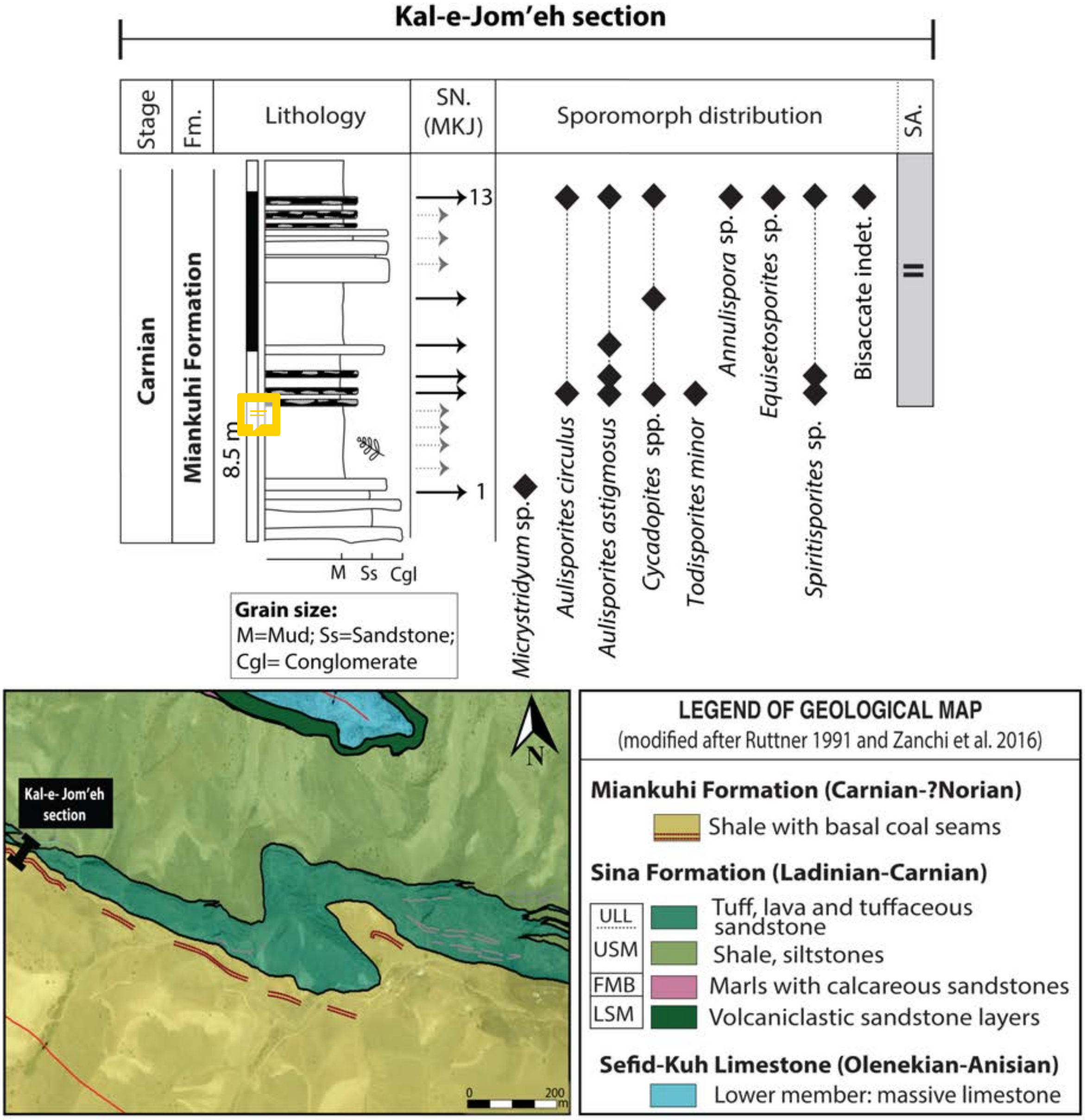

Fig. 5. Lithostratigraphy of the Triassic (Carnian) Miankuhi Formation from the Kal-e-Jom'eh section, Aghdarband, with the re-drawn geological map of the area surrounding the studied section and distribution of sporomorph assemblages. Black arrows indicate the palynological-productive samples. Abbreviations: Fm: Formation; SN: Sample number; SA: Sporomorph assemblage.

fern (*Deltoidospora* sp.) and sphenophyte (*Calamospora* sp.) spores. This assemblage suggests a late Ladinian age, which is in agreement with the age suggested by Balini et al. (2019) based on ammonoid and bivalves.

Assemblage II is characterized by the first occurrence of *Aulisporites astigmosus*, *A. circulus*, and *Spiritisporites spirabilis* together with the persistence of the spores typical for assemblage I. Assemblage II has been identified in the lowermost part of the Miankuhi Formation in the upper Kal-e-Faqir composite section, in the Kal-e-Bast section, and the Kal-e-Jom'eh section. This assemblage is characterized by the co-occurrence of sphenophyte (*Equisetosporites* sp.) and bryophyte (*Annulispora* sp.) spores and bennettitalean, cycad, and ginkgophyte (*Aulisporites astigmosus*) pollen, as well as conifer pollen grains (*Spiritisporites* spp.). The composition of this assemblage supports the latest early Carnian to late Carnian age corresponding to the Carnian Pluvial Episode for the lower part of the Miankuhi Formation (Mazaheri-Johari et al., 2021).

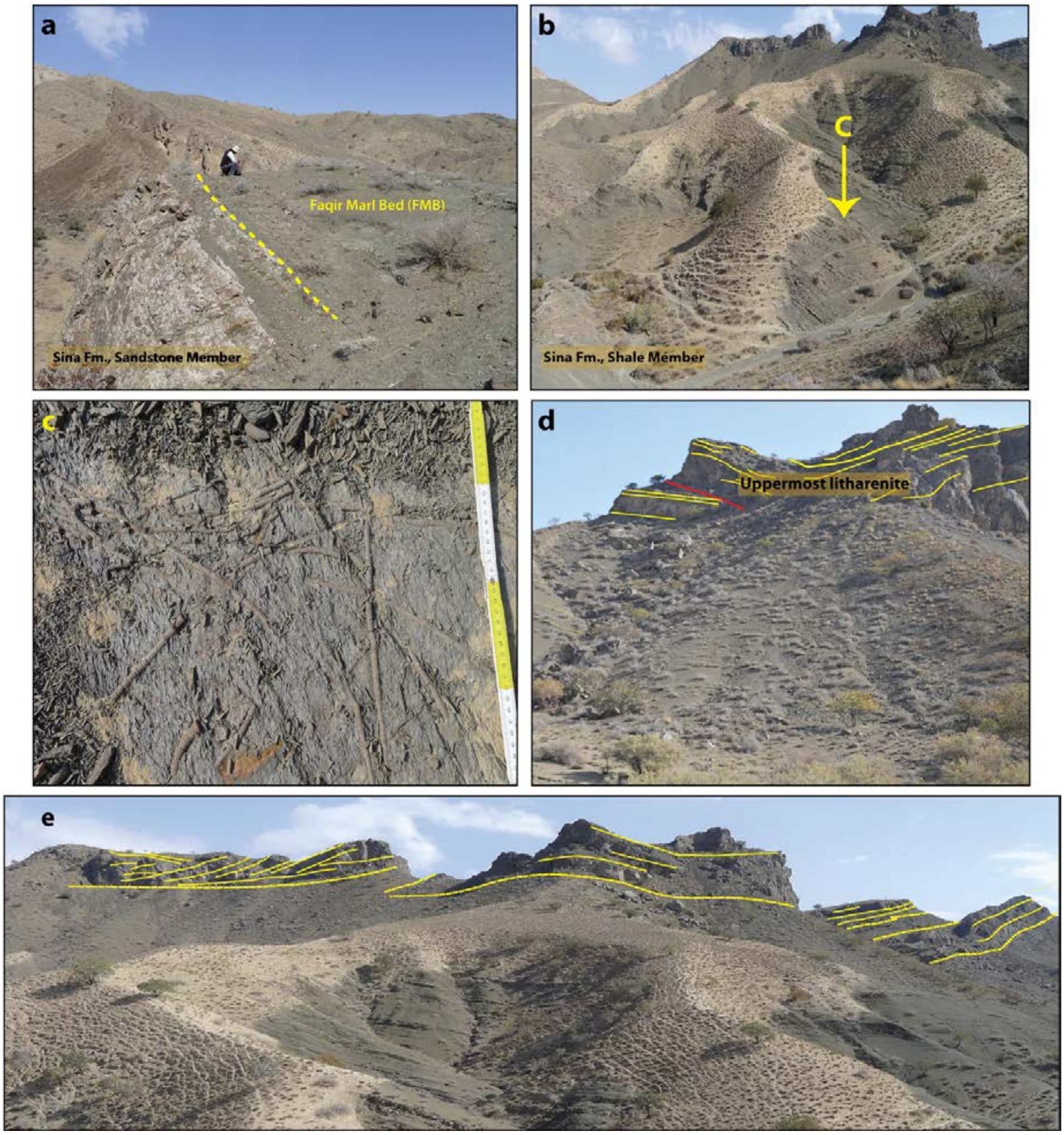

Fig. 6. (a) The transition from the upper part of the Lower Sandstone Member of the Sina Formation to the Faqir Marl Bed (FMB). **(b)** Above the FMB, the Upper Shale Member (USM) crops out, characterized by a very thick siliciclastic succession with the fining and thinning upward trend (Upper Shale Member). **(c)** Several pelagic crinoids were found in some layers of the Upper Shale Member. **(d)** The Upper Litharenite lithofacies (ULL) at

the topmost USM. **(e)** The transition of Upper Shale Member (USM) to the Upper Litharenite lithofacies (ULL) is visible both upward and laterally.

6.3. Quantitative analyses

The quantitative composition varies noticeably between the two main palynological assemblages. Due to the state of preservation of the sporomorphs it was not possible to construct a quantitative trend curve but only to give a semi-quantitative indication on the different assemblages (Fig. 8). Semi-quantitative analyses were carried out for sample FQ4 from the Sina Formation of the Kal-e-Faqir composite section. Four samples were rich enough in sporomorphs for quantitative palynological assemblages in the Mihankui Formation, two samples come from the Kal-e-bast section (samples KB2 and KB4) and two others from the Kal-e-Jom'eh section (samples MKJ6 and MKJ13) (Fig. 8).

Assemblage I (yellow in Fig. 8) is dominated by bisaccate pollen (33 %) and indeterminable spores (25 %). Trilete spores (12 %) and *Cycadopites* (12 %) are relatively common, whereas all other taxa and sporomorph groups are rare. This pattern of vegetation reflects a flora well balanced between typical xerophytic elements such as bisaccate pollen of seed ferns and conifers (*Triadispora* sp., *Lunatisporites* sp., *Araucariacites* sp.) and typical hygrophytic elements such as those represented by trilete (12%) or indeterminable spores (25 %) (Fig. 8).

Assemblage II (in greenish in Fig. 8) is generally dominated by trilete (29–45%) and indeterminable spores (22–57 %). *Cycadopites* pollen (6-33%) are abundant, whereas bisaccate pollen (0–3%) are extremely rare or completely absent in the assemblages. *Aulisporites* types of pollen occur at a very variable abundance, from 0% to 30%. In the assemblage MKJ 6, this is slightly different with *Cycadopites* being the dominant element (33%) followed by *Aulisporites astigmosus* (30%), indeterminable spores (27%), trilete spores (8%), and *Spiritisporites* (2%). From a vegetational point of view, the hygrophytic elements dominate this assemblage completely, with even the gymnosperms being mainly represented by hygrophytic elements (e.g., Bennettitales, cycads, and/or ginkgophytes) (Fig. 8).

7. Discussion

7.1. Stratigraphy and tectonics

The Aghdarband Basin in the Kopeh-Dagh Range (NE Iran) has recently attracted huge interest for unraveling the Triassic evolutionary dynamics and tectonic evolution of the southern margin of the Laurasia during the final closure of the Paleotethys Ocean and the accretion of Cimmerian terranes to southern Laurasia. Our new data make it possible to refine the stratigraphy of the studied interval and consider it in terms of basin evolution in a regional context.

The local occurrence of the monogenic conglomerate in the Lower Sandstone Member of the Sina Formation (Balini et al., 2019) overlapping the basal unconformity suggests sedimentation through mass flow processes in marine depocenters, adjacent to topographically higher areas of bypass or where the Lower Triassic to Anisian substrate was still subjected to erosion. The following thick-bedded, mainly volcanoclastic sandstones were deposited by turbidite currents in a relatively deep-marine environment. The lower part of the LSM can be interpreted as the product of submarine sedimentation during regression in an overall back-arc, tectonically active setting. The middle part of LSM, commonly characterized by tuffaceous shale layers, is interpreted as the result of a transgression, whereas the thickening and the coarsening-upward stack of litharenite beds at the top of the LSM represent a prograding sandstone lobe leading to the development of a shallower marine setting. The transition to the FMB is marked by a condensed, ammonoid-bearing surface that has been interpreted by some authors (Balini et al., 2019) as a drowning unconformity. Baud et al. (1991) interpreted the following-up marls and calcareous shales as the product of sedimentation in a distal, deep ramp environment. However, the transition from FMB to USM can be referred to as a further deepening of the depositional setting, governed by siliciclastic sedimentation and turbidity flow processes. The following-upward succession is characterized by a thinning and fining upward trend that could be related to a general transgression, limited upward by a maximum flooding interval, just a few tens of meters below the ULL. Well bedded, laminated to massive sandstones, and shaly to silty intercalations composing the basal part of this last unit are organized in a thickening/coarsening upward stack and pass upwards to clinostratified and amalgamated beds of litharenite. The overall spatial distribution and organization of the facies associations suggest a transition from a prodelta to a delta slope and then to a delta front setting. Indeed, erosive channels with accretionary bars recognized in the uppermost part of the ULL could represent distributary channels, while some shaly intercalations lying laterally eastward to the sandstone bodies can be referred to interdistributary bay deposits. Moreover, in an overall view, the ULL is organized in at least three sandstone bodies (Fig. 6E) laterally pinching out to prodelta shales and siltites, with the latter (upper) litharenitic body extended almost on the whole area.

The transition from the Sina Formation to the Miankuhi Formation marks an important sequence boundary. Field observations often show an erosional surface covered by a basal layer of polygenic conglomerates and intercalated sandstones. Alternations of sandstone channels and pelites characterize the initial part of the Miankuhi Formation and can be framed in a distal alluvial plain environment, with common terminal splays and overbank deposits. Fine-grained conglomerates often occupy the lower central part of channels, overlapped by coarse-grained festooned sandstones (Fig. 7a), laterally passing to cross-bedded sandstones representing lateral accretionary sand bars, and upward grading to reddish fine sandstones and siltites. The closeness of channels in the vertical stacking pattern points to low accommodation space for the initial part of the Miankuhi Formation. However, the unit changes upwards to prevailing pelites intercalated with small channels, suggesting an increase in accommodation rates. Moreover, the occurrence of oligotrophic foraminifers, hydromorphic paleosols, and the coal layers point to the depositional environment shifts towards a marginal marine setting, with a coastal mudflat periodically flooded by the sea and by rivers and rich in paralic swamps where the organic material accumulated. The coal layer can record the decreasing of base sea level rise, and the maximum flooding interval (cf. Catuneanu, 2006). Therefore, about fifty meters of Miankuhi Formation can be framed in a general transgressive trend, the coal interval seems to record the balance between sea level rise and river discharge, then a regressive trend is recorded by the sandstone layers. Above this, the shale-dominated intervals can be interpreted as a transgression.

The deformation of Miankuhi beds during an intense compressional event caused a significant uplift (Zanchi et al., 2016), giving origin to the upper unconformable boundary of the Miankuhi Formation covered by the Middle Jurassic strata (Kashaf-Rud Formation). The recorded unconformity at the base of the Ghal'eh Qabri Shales, Bajocian in age, may therefore correspond to the so-called "Mid-Cimmerian event" (cf. Seyed-Emami et al., 2021). The post-collisional Mid-Cimmerian tectonic event occurred across the Iran Plate (Central Iran and Alborz mountains of northern Iran) and Turan domain and it has been related to the opening of the Paleo-Caspian basin to the north (Fürsich et al., 2009b).

Hence, the unconformity between the Sina and the Miankuhi formations could have a tectonic origin related to the faraway effect of the first stages of the Eo-Cimmerian collision strongly enhanced by sedimentary dynamics and/or the climatic driver, which the latter is the main candidate for this scenario.

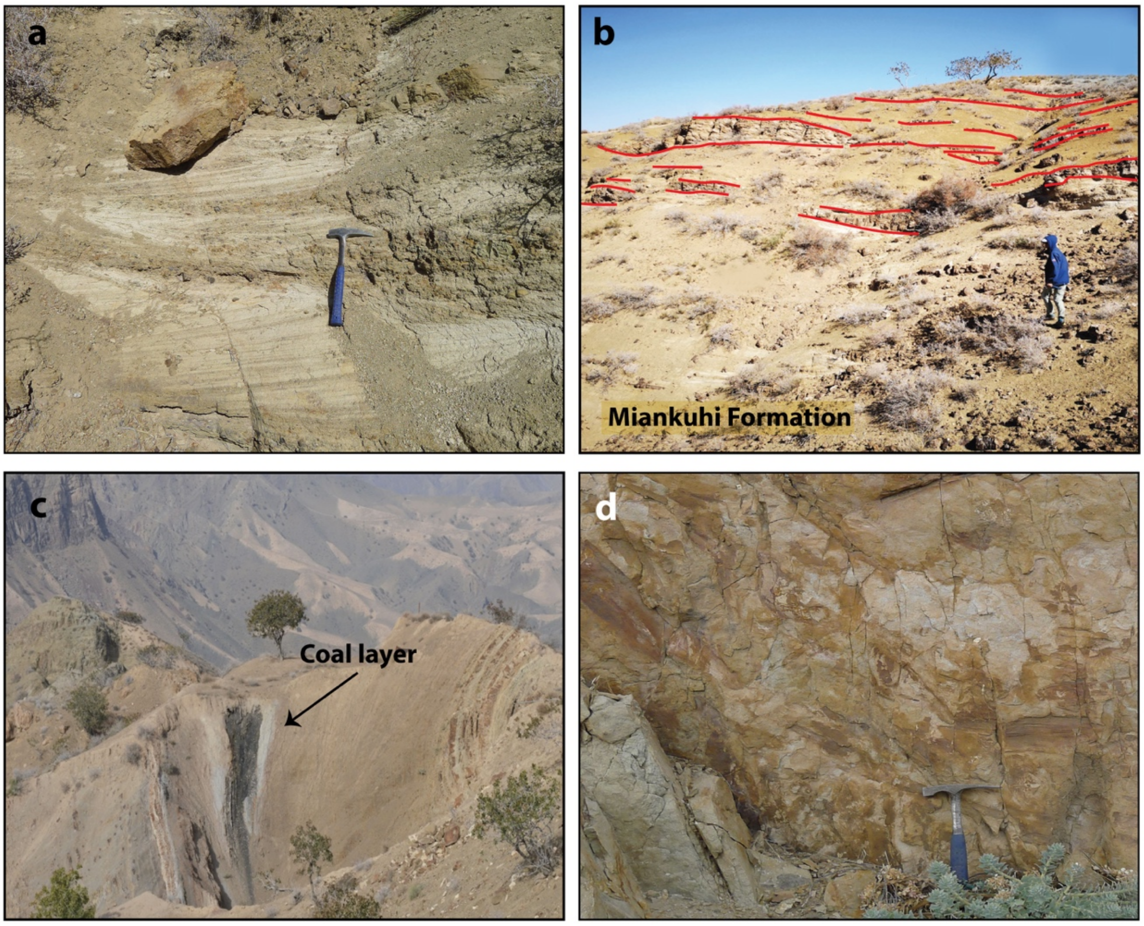

Fig. 7. (a) Cross bedded sandstones in the lowermost Miankuhi Formation. **(b)** Erosive channels in the Miankuhi Formation. **(c)** Basal Coal layer of the Miankuhi Formation. **(d)** Plant-bearing intervals of Miankuhi Formation.

7.2. Facies and basin evolution

After a significant tectonic phase disrupting the middle Anisian paleotopography of the Aghdarband Basin, uplifting several sectors and eventually developing structural highs and more subsiding areas (Balini et al., 2019), a deep basin environment with common turbidite currents developed in the Ladinian. This deep basin was filled by the volcanoclastics of the Sina Formation and the progressive basin infilling was controlled by the relative sea-level oscillations, related both to eustatic variations and to persisting active tectonics. In the western part of the Aghdarband Basin, a major phase of basin infilling started in the latest Ladinian, leading to a progressive decrease in sedimentation depth and a sedimentary environment transition from offshore to delta setting, then to a shallow marginal marine, and finally to a mainly fluvial setting. Notably, there could be a good correlation between the transgressive-regressive trends described for the latest Ladinian and the depositional trends reported from several regions of the Tethys area, such as the Dolomites (cf. depositional sequence La 2 in

Hardenbol et al., 1998; Gianolla et al., 1998, 2021; TLa3 in Haq, 2018) (Fig. 9). According to our data, there is a shallow depositional environment before reaching the boundary between the Sina and the Miankhui formations. The lower boundary of the latter unit has, therefore, been placed tens of meters below the original one reported by Ruttner (1991) for the western sector, starting from the basal conglomerates of the Miankhui Formation (Mazaheri-Johari et al., 2021). The subsequent relative sea-level drop helped to establish an opportunity to erode early Julian depositions. In a shallow environment with gentle topography, the shoreline would move some hundreds of meters seawards in response to the sea-level fall, resulting in a substantial subaerial (and fluvial) exposure and erosion of the previously deposited sediments. The erosive channels in the lower part of the Miankuhi Formation would locally cut each other and erode older sediments, including upper parts of the Sina Formation, in a vertical direction. In addition, the unconformity at the base of the Miankuhi Formation could represent a time gap of about two million years at most (see the Biostratigraphy section), which is not such a large time gap as reported in other studies (Ruttner, 1991; Seyed-Emami, 2003; Zanchi et al., 2016; Balini et al., 2019; Liaghat et al., 2021). A significant sea-level drop during the CPE is documented worldwide (e.g., Roghi et al., 2010; Stefani et al., 2010; Arche and López-Gómez, 2014; Mueller et al., 2016a; Gattolin et al., 2015; Franz et al., 2014; Zhang et al., 2015; Shi et al., 2017; Barrenechea et al., 2018; Davies and Simmons, 2018; Klausen et al., 2020) and this enhanced erosion could be associated with this global sea-level fall. After the flattening of the basin, a general transgressive trend is documented by the Miankuhi Formation: this marginal marine interval is the only unit of the Aghdarband Group that can be found outside the Aghdarband tectonic window. The wide areal distribution of the Miankuhi Formation may thus represent an important large-scale basin reorganization affecting the whole back arc region of the upper plate accompanied by a general cessation of volcanic activity, both induced by the consequences of the Cimmerian orogeny. It is worth mentioning that this important transgression phase (Fig. 9) is similar to those observed during the late Carnian in most of the Tethyan successions (e.g., Lehrmann et al., 2005; Xu et al., 2014; Sun et al., 2016; Caggiati et al., 2018).

The reinterpretation of the stratigraphic and sedimentological patterns in this study allowed us to reconsider the extent of the unconformity strictly related to the Cimmerian event, both in terms of sedimentary and time gap.

7.3. Palynological evolution

Assemblage I (upper part of the Sina Formation) can tentatively be correlated with late Ladinian–early Carnian associations dominated by trilete spores in association with various species of *Lunatisporites*, *Triadispora,* and *Ovalipollis* (Mietto et al., 2012; Van der Eem, 1983).

Assemblage II (lowermost Miankuhi Formation) can be correlated with the *Aulisporites astigmosus* assemblage of Roghi et al. (2010), which is Julian 2 in age. *Aulisporites astigmosus* is a biostratigraphic marker and has been reported from many palynological assemblages corresponding to the CPE including the Veszprém Formation from the Balaton Highland (Hungary: Baranyi et al., 2019) and the Raibler Schichten in the Northern Calcareous Alps (Italy: Kavary, 1966; Jelen, 1982; Roghi et al., 2010). In the Cave del Predil area (Julian Alps, Italy), *Aulisporites astigmosus* is typical for the Rio del Lago Formation and the Tor Formation (Roghi, 2004; Dal Corso et al., 2018). The same palynological composition is documented in the Heiligkreuz Formation in the Dolomites (Praehauser-Enzenberg, 1970; Roghi et al., 2010; Breda et al., 2009). A rich association of *A. astigmosus*, *Cycadopites,* and fern spores also occur in some layers of the Schilfsandstein (Stuttgart Formation) in Germany (Visscher et al., 1994; A assemblages of Franz et al., 2019). The Schilfsandstein of Poland is dominated by an assemblage with *Aratrisporites, Calamospora,* and *Aulisporites* (Fijałkowska-Mader, 1999).

In the Boreal Realm, *Aulisporites astigmosus* was found in the lower parts of the Tschermakfjellet Formation (Vigran et al., 2014; Mueller et al., 2016b), within the Tethyan *T. aonoides* ammonoid zone, so in slightly older sediments in comparison with the southern Tethyan realm. This was interpreted as a diachronous occurrence of the *A. astigmosus* zone, appearing for the first time in the Boreal region and later moving towards the south into the peri-equatorial region. The most plausible hypothesis suggests that the *Aulisporites*-producing mother-plant, a hygrophytic gymnosperm (Bennettitales, Kräusel and Schaarschmidt, 1966; Balme, 1995) migrated southwards during the Carnian Pluvial Episode due to the more humid palaeoenvironmental conditions in a generally semi-arid to seasonal tropical climate of the circum-Tethys realm.

Circumpollen grains and cavatomonolete spores (*Aratrisporites*), typical for the *Duplicisporites continuus* assemblage of Roghi (2004) and the *Aulisporites-Aratrisporites* acme (Roghi, 2004), are present at lower latitudes in the Arabian Plate (NE Iraq, Baluti Formation) (Lunn, 2020) but are very rare (3%) in our studied interval. Noticeably, the palynological association discovered in Iraq resembles the palynological associations of the Alpine Realm rather than our assemblages from Aghdarband Basin.

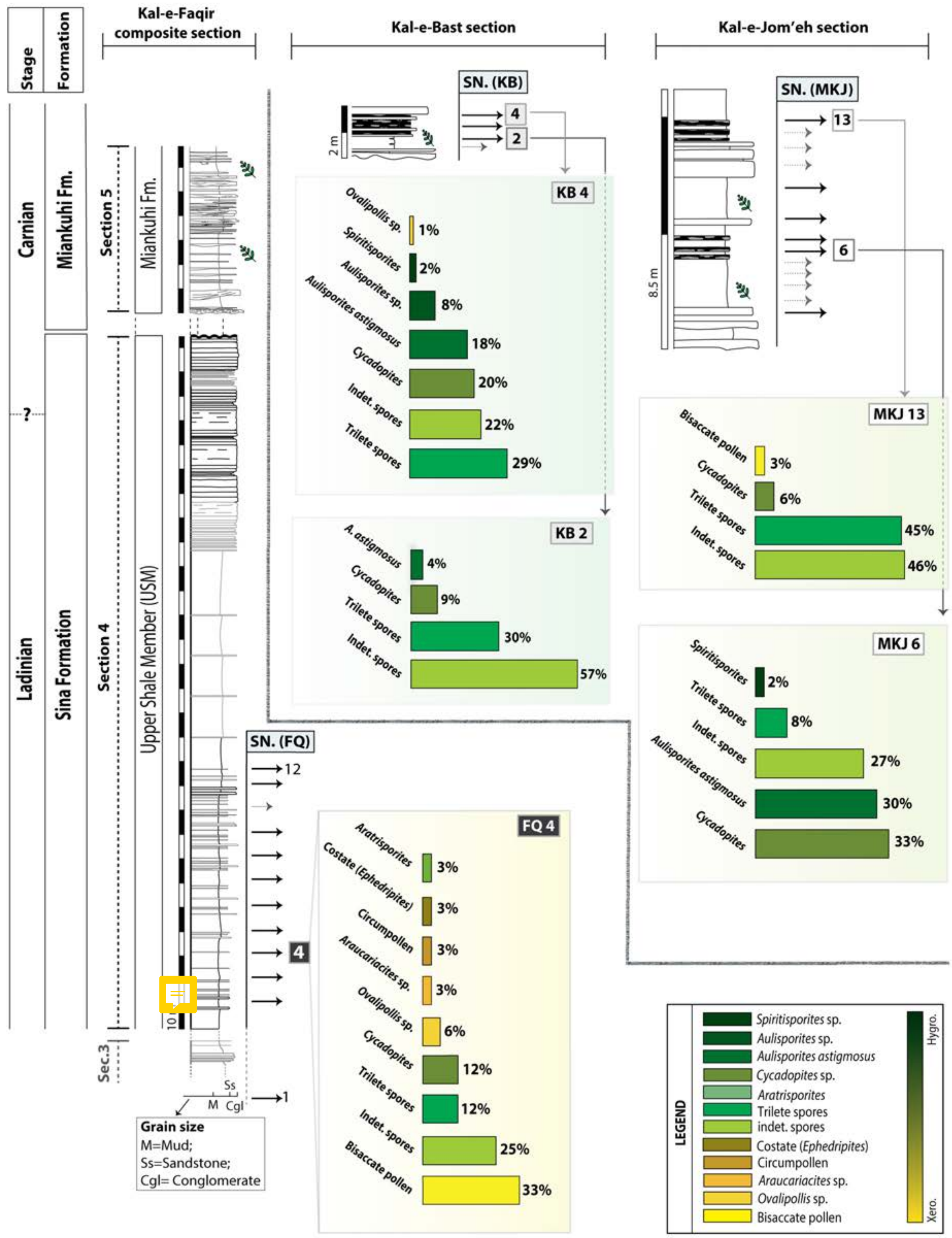

Fig. 8. Quantitative results of discovered palynomorphs from uppermost Sina Formation in the Kal-e-Faqir composite section (FQ4 sample), and lowermost Miankuhi Formation in the Kal-e-Bast (KB2 and KB4 samples) and Kal-e-Jom'eh (MKJ6 and MKJ13 samples) sections. Greenish colors indicate hygrophytic elements and

yellowish ones show xerophytic sporomorphs. Abbreviations: Fm: Formation; SN: Sample number; Sec. 3: section 3; *A. astigmosus*: *Aulisporites astigmosus*; Indet: indetermined.

The bad preservation withstanding, the two assemblages show quite different quantitative records reflecting different local environments and local vegetation. Although hygrophyte elements such as trilete spores (12 %) and indeterminable spores (25%) are already well present

Plate I

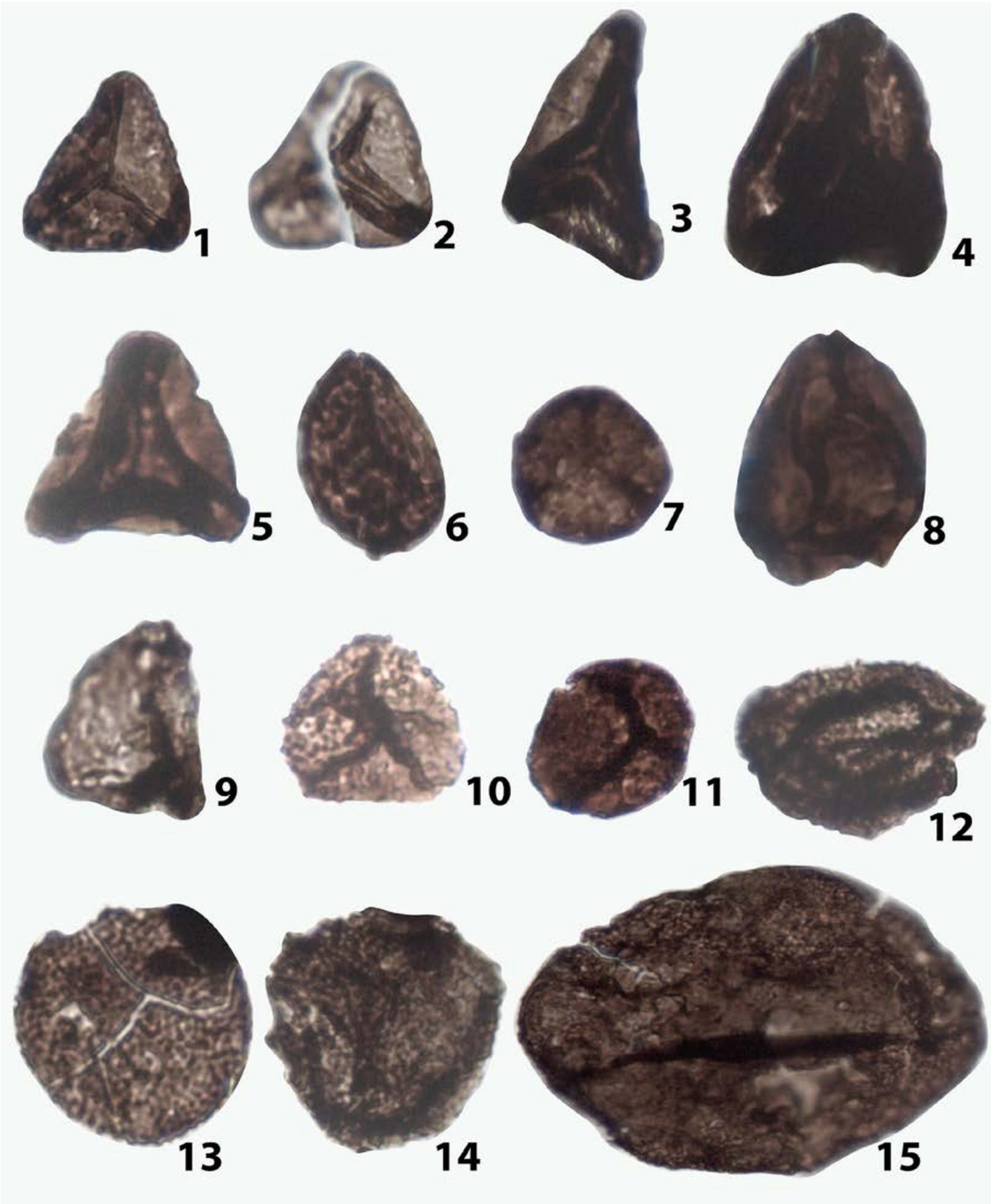

Plate I. Sporomorphs of the plant horizon. Each taxon name is followed by the section name, sample number, slide number, scale, and stage coordinates for a Leica DM750 light microscope. **1–2)** *Concavisporites* sp.; 1: Kal-e-Bast section; KB 3; Slide II; 27 µm high; U58/1; 2: Kal-e-Bast section; KB 3; slide I; 28 µm high; P26/2; **3)** *Concavisporites toralis*; Kal-e-Bast section; KB 4 I; slide II; 42 µm high; V68/4; **4)** *Kyrtomisporis leavigatus*; Kal-e-Bast section; KB 4I; slide II; 38 µm high; J63/2; **5)** *Dictyophyllidites mortonii*; Kal-e-Bast section; KB 4I; slide I; 30 µm diameter; R75; **6)** *Lycopodiacidites kokenii*; Kal-e-Bast section; KB 4I; slide II; 25 µm diameter; W5; **7)** *Retusotriletes hercynicus*; Kal-e-Bast section; KB 4I; slide I; 31 µm diameter; J74/2; **8–9)** *Deltoidospora* sp.; 8: Kal-e-Faqir section; Fq 8; slide I; 40 µm high; N53/3; 9: Kal-e-Bast section; KB 4 I; slide I; 35 µm high; X67; **10)** *Lunzisporites* sp.; Kal-e-Bast section; KB 4 I; slide I; 27 µm diameter; Y67; **11)** Cf. *stereisporites* sp.; Kal-e-Faqir section; Fq 8; slide V; 24 µm diameter; G62/2; **12)** *Araucariacites* sp. Kal-e-Bast section; KB 4 I; slide I; 33 µm diameter; W58/2; **13–14)** *Spiritisporites* cf. *spirabilis*; Kal-e-Bast section; 13: KB 2; slide II; 35 µm diameter; L31; 14: KB 4 I; slide II; 33 µm diameter; M23/4; **15)** Ind. foveolate trilete spore; Kal-e-Faqir section; FQ 8; slide IV; 95 µm high; H45/1.

in the Sina Formation, bisaccate pollen is still an important element of the flora (33%). The sporomorphs of the Miankuhi Formation, on the other side, are completely dominated by hygrophytic elements, both trilete and indeterminable spores, but also hygrophytic markers among the pollen grains such as *Aulisporites* and *Cycadopites* (Fig. 8). This, as well as the presence of coaly layers, cannot be explained only by a sea-level shift and paleoenvironmental change but the extent of the changes supports a change in the climate signal. Furthermore, the biostratigraphic markers provide additional support for the correspondence of the base of the Miankuhi Formation to the CPE.

7.4. Age consideration

A U-Pb zircon age of 217.1 ± 1.7 has been obtained for a large magmatic body (Torbat-e-Jam Granite) intruding the deformed terrigenous succession attributed to the Miankuhi Formation at about 50 km to the east of Aghdarband, in the north of Torbat-e-Jam (Zanchetta et al., 2013). This suggests the Norian as a minimum age for the timing of the inversion and deformation of the Miankuhi Formation. The dinoflagellate cyst assemblage (*Hebecysta, Heibergella, Rhaetogonyaulax, Sverdrupiella*) reported from this formation and considered Norian in age, is largely corroded and badly preserved, making the species-level identifications tentative (Ghasemi-Nejad et al., 2008). Moreover, the described dinoflagellate cysts are not exclusively restricted to the Norian but reach down to the Carnian (e.g., Wiggins, 1973; Bujak and Fisher, 1976; Riding et al., 2010; Mangerud et al., 2019; Mantle et al., 2020) and some of them have been found in the Raibl Group from the Eastern Swiss Alps (Hochuli and Frank, 2000). The palynological analyses support an assignment of the basal Miankuhi Formation to the latest early to late Carnian age (see above) and there is no clear evidence for a Norian age of the entire Miankuhi Formation in the studied area.

Plate II

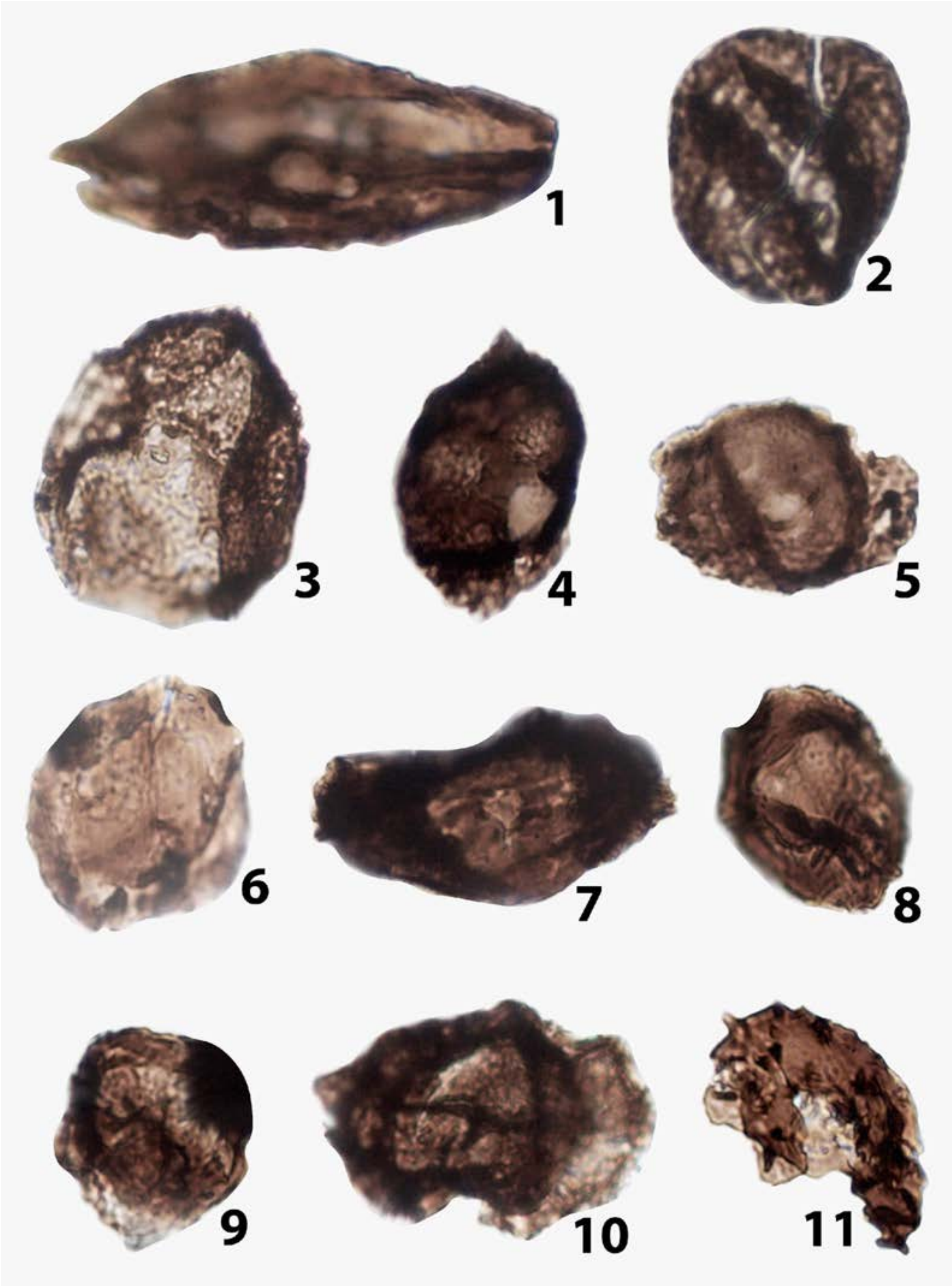

Plate II. 1–3) *Cycadopites* sp.; 1: Kal-e-Faqir composite section; Fq 4; slide II; 26 μμ high; K42/2; 2: Kal-e-Bast section; KB 4 II; slide II; 30 μm diameter; U6/3; 3: Kal-e-Jom'eh section; MKJ 9; slide II; 56 μμ high; R74; **4)** cf. *Triadispora* sp.; Kal-e-Faqir composite section; Fq 4; slide I; 37 μm high; B48/1; **5)** *Triadispora* sp.; Kal-e-Faqir composite section; Fq 8; slide I; 36 μm high; H29; **6)** *Annulispora* sp.; Kal-e-Jom'eh section; MKJ 13; slide

V; 46 µm diameter; M44/4; **7)** *Lunatisporites* sp.; Kal-e-Faqir composite section; Fq 4; slide I; 29 µm high; P42/2; **8–9)** Circumpolles; Kal-e-Faqir composite section; 8: Fq 4; slide I; 37 µm diameter; R37/2; 9: Fq 8; slide I; 35 µm diameter; O52/4; **10)** *Chordasporites* sp.; Kal-e-Faqir section; Fq 8; slide II; 34 µm high; N49; **11)** *Baculatisporites* sp.; Kal-e-Faqir section; Fq 8; slide II; 50 µm high; J35/3.

7.5. The CPE in the north-eastern margin of the Tethyan Realm

The fluvial sediments govern the depositional pattern of the lowermost Miankuhi Formation with plant-bearing marls and histosol horizons that likely developed under humid environmental conditions. The prevalence of relative humid paleoclimate and/or environment can be deduced from the composition of the plant community (including sphenophytes, ginkgophytes, conifers, and *incertae sedis*) at this site and in the surrounding areas (Boersma and Van Konijnenburg-van Cittert, 1991; Mazaheri-Johari et al., 2021). The morphospecies groups of palynomorphs evidence a clear shift towards hygrophytic elements in the lowermost Miankuhi Formation and reflect the expansion of wet habitats on the continent during the latest early Carnian to late Carnian age. The observed sedimentological and palynological patterns as well as plant fossil assemblages show a close resemblance to those observed during the humid phases that mark the Carnian Pluvial Episode in many stratigraphical sections worldwide. This episode of global climate change dated from the Julian 2 (early Carnian) to the Tuvalian 2 (late Carnian) and is comprised of several humid pulses (Breda et al., 2009; Kozur and Bachmann, 2010; Stefani et al., 2010; Dal Corso et al., 2015, 2018; Baranyi et al., 2018, 2019) coupled to substantial changes in marine and terrestrial ecosystems (e.g., Dal Corso et al., 2020). On land, paleobotanical and palynological investigations from different latitudes revealed a shift of floral associations towards the elements with a high preference for humid conditions (e.g., Roghi et al., 2010; Preto et al., 2010; Mueller et al., 2016b; Baranyi et al., 2018, 2019; Fijałkowska-Mader et al., 2021).

Plate III

Plate III. 1) *Baculatisporites* sp.; Kal-e-Bast section; KB 4 I; slide I; 32 µm diameter; Q63/2; **2)** *Asseretospora* sp.; Kal-e-Bast section; KB 4 I; slide I; 38 µm diameter; X71/2; **3–5)** *Aulisporites astigmosus;* Kal-e-Bast section; 3: KB 2; slide I; 60 µm diameter; Q18/4; 4: KB 4 I; slide I; 60 µm length; Y60/4; 5: KB 4 I; slide II; 35 µm length; V45; **6–7)** *Aulisporites circulus;* 6: Kal-e-Bast section; KB 4 I; slide I; 31 µm diameter; M64; 7: Kal-e-Jom'eh section; MKJ 6; Slide I; 25 µm diameter; L66; **8–9)** *Cycadopites* sp.; Kal-e-Bast section; 8: KB 4 I; slide I; 34 µµ diameter; V67/3; 9: KB 4 I, slide I; 39 µm diameter; T66/3; **10)** *Trachysporites* sp.; Kal-e-Bast section; KB 4 I; slide I; 30 µm diameter; F25/4; **11)** *Todisporites* sp.; Kal-e-Bast section; KB 4 I; slide I; 40 µm diameter; T40; **12)** *Todisporites minor*; Kal-e-Jom'eh section; MKJ 6; slide I; 35 µm diameter; G68/3; 1**3)** *Ephedripites* sp.; Kal-e-Faqir section; Fq 4, slide I; 47 µm diameter; F54/1; **14)** *Ovalipollis* sp.; Kal-e-Faqir section; Fq 1; slide 0II; 38 µm high; R34/1; **15)** *Calamospora* sp.; Kal-e-Faqir section; Fq 1; slide 0II; 37 µm high; X44/3.

The CPE has been detected in the adjacent area, NE Iraq in the Arabian Plate, where abundant siliciclastics were deposited (shale B1 from Member B of Kurra Chine Formation: see discussion in Lunn, 2020; Hanna, 2007; Lunn et al., 2019; Davies and Simmons, 2020; Lunn, 2020) (Fig. 9). In the Eurasian Plate, along the northern foothills of the Turkestan-Alai Range (SW Kyrgyzstan), a thick succession of clastic sediments, the Madygen Formation, accumulated in a lush vegetated fresh-water basin under humid to semi-humid climatic conditions (Berner et al., 2009; Moisan et al., 2012, 2021). The flora of the Madygen Formation (several types of bryophytes, horsetails, lycopsids, ferns, ginkgophytes, pteridosperms, and conifers) resembles those from the CPE (Kustatscher et al., 2018). This formation seems to be slightly younger than mid-Carnian in age (the base of the unit gives a ~237± 2 Ma) and records the development of a large endorheic freshwater basin nested on continental Laurasia. Interestingly, the appearance of freshwater lakes is one of the main features of the CPE in continental settings. Except of some not well-constrained bauxite deposits from the Middle Triassic Kani Zarrineh (NW Iran) in the Irano-Himalayan belt (Abedini et al., 2021) (Fig. 9), there are no clear records of CPE from other parts of the Iran region (Iran plate) due to the late Carnian to early (?)Norian sedimentary gap, and in some places even younger, in response to the Cimmerian collision and subsequent uplift and erosion (Seyed-Emami, 2003; Fürsich and Hautmann, 2007; Fürsich et al., 2009a; Zanchi et al., 2009a; Krystyn et al., 2019) (Fig. 9). In the Nakhlak area (Central Iran), the top of the Ashin Formation reaches at most the early Carnian but is mainly late Ladinian in age (Balini et al., 2009), so there is no sedimentary record, up to now, of upper Triassic strata under the Cretaceous unconformity. In Central Iran, according to Krystyn et al. (2019), a distinct unconformity separates the Shotori Formation from the Espakh Limestone. Despite poor age control, the top of the Shotori Formation should be early Carnian in age (Krystyn et al., 2019). According to these authors, the demise of the Carnian carbonate platform should be related to the general demise of the carbonate microbial platform documented Tethys-wide during the CPE (Jin et al., 2020) but more studies are needed to prove this assumption.

7.6. CPE or Cimmerian Orogeny, the controversy

During the Late Triassic, the Turan domain as part of the southern margin of Laurasia was located in a relatively stable position at about ~35°N (Besse et al., 1998; Muttoni et al., 2009, 2015; Mattei et al., 2015; Garzanti and Gaetani, 2002; Barrier et al., 2018) and therefore, the observed change towards humidity (from xerophytic to hygrophytic assemblages) could not be related to a change in paleolatitudinal position. The short duration of the CPE (lasted for

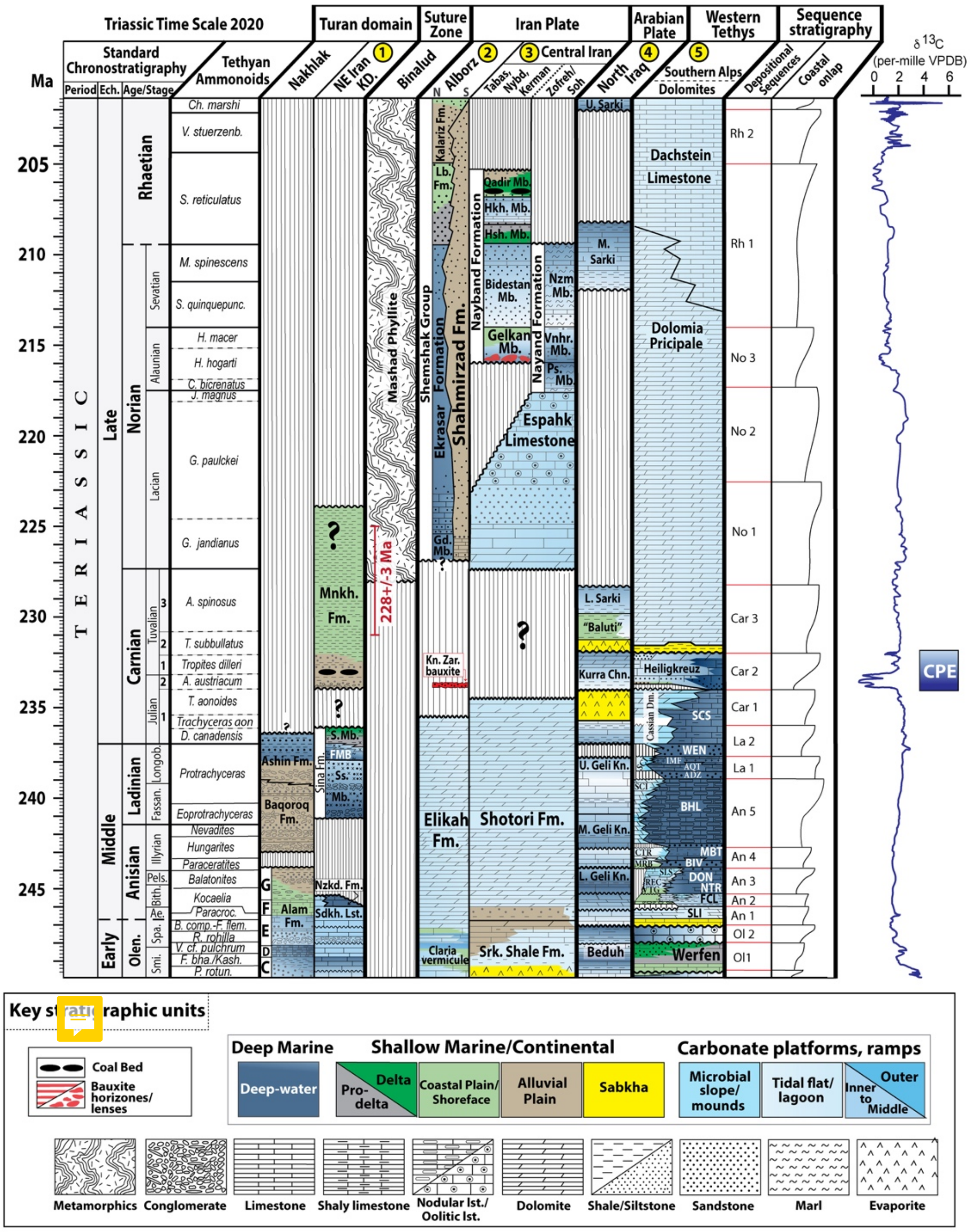

Fig. 9. Lithostratigraphy of Triassic rock units from Iran region (Turan domain and Iran Plate), NE Iraq as part of the Arabian Plate (modified after Seyed-Emami, 2003; Fürsich and Hautmann, 2007; Fürsich et al., 2009b; Seyed-Emami et al., 2009; Balini et al., 2009; Krystyn et al., 2019; Liaghat et al., 2021; Lunn et al., 2019, Davies and Simmons, 2020; Tamar-Agha et al., 2020), and Western Tethys (Southern Alps, Dolomites; modified from Mietto et al., 2020). Yellow numbers are the same as in figure 2. Ammonoid zones from Bernardi et al. (2018). Sequence stratigraphy after Gianolla and Jacquin (1998), Hardenbol et al. (1998), Gianolla et al. (1998, 2021). Composite organic carbon-isotope curve modified from Triassic Time scale 2020 (Ogg et al., 2020). Abbreviations: Ech. Epoch; Olen: Olenekian; Smi: Smithian; Spa: Spathian; Ae: Aegean; Bith: Bithynian; Pels: Pelsonian; Fassan: Fassanian; Longob: Longobardian; Fm: Formation; Mb: Member; Sdkh. Lst: Sefidkuh Limestone; Nzkd: Nazar-kardeh; Ss: Sandstone; FMB: Faqir Marl Bed; S. Mb: Shale Member; Mnkh. Fm: Miankuhi Formation; Kn. Zar: Kani Zarrineh; KD: Kopeh-Dagh; Nybd: Nayband area; Gd: Galanderud; Lb: Laleband; Srk. Shale: Sorkh Shale;

Hsh: Howz-e-Sheikh; Hkh: Howz-e-Khan; Ps: Parsefid; Vnhr: Venher; Nzm: Niazmargh; L. Geli Kn: Lower Geli Khana; M. Geli Kn: Middle Geli Khana; Kurra Chn: Kurra Chine; L. Sarki: Lower Sarki; M. Sarki: Middle Sarki; U. Sarki: Upper Sarki; SLI: Lower Serla Dolomite; FCL: Coll'Alto dark Limestones; NTR: Monte Rite Formation; DON: Dont Formation; VTG: Voltago Conglomerate; REC: Recoaro Limestone; SLS: Upper Serla Formation; BIV: Bivera Formation; MRB: Richthofen Conglomerate and Morbiac dark Limestone; MBT: Ambata Formation; CTR: Contrin Formation; SCI: Sciliar Formation; BHL: Livinallongo/Buchenstein Formation; ADZ: Zoppè Sandstone; AQT: Acquatona Formation; IMF: Fernazza Formation; WEN: Wengen Formation; SCS: San Cassiano Formation.

1.2–1.6 Myrs) (e.g., Zhang et al., 2015; Miller et al., 2017; Bernardi et al., 2018; Colombi et al., 2021), its global records in many different stratigraphic successions, the global carbon cycle disruption marked by sharp negative carbon-isotope excursions (NCIEs) (Dal Corso et al., 2012, 2015; Mueller et al., 2016b; Sun et al., 2016; Miller et al., 2017) during Carnian, and the pulses of increased mercury loading in the Western Tethys during the CPE (Mazaheri-Johari et al., 2021), as well as other geochemical proxies (Xu et al., 2014; Tomimatsu et al., 2021), suggest a link between pulses of Wrangellia Large Igneous Province (LIP) and/or other coeval volcanisms (Furin et al., 2006; Sun et al., 2016; Dal Corso et al., 2012, 2020; Fu et al., 2020; Li et al., 2020), NCIEs, and the CPE environmental perturbations. These data bring into question the interpretation of the CPE as a direct consequence of the Cimmerian Orogeny proposed by some researchers (e.g., Hornung et al., 2007; Krystyn et al., 2019; Chu et al., 2021). Hornung et al. (2007) explained the mid-Carnian climatic perturbation (CPE) by the collision of the Cimmerian terranes with Laurasia, and the uplift of the Cimmerian Orogen. This new mountain chain forced the monsoonal circulation system to enhance precipitations, weathering, erosion, and run-off. But it seems unlikely that the global climatic perturbation recorded by the CPE is linked to the collision of a relatively small microcontinent with Laurasia (Şengör, 1984), since the effects of this uplift should be more prolonged in time instead the CPE climatic perturbation is very limited in time as in the Tuvalian, globally, there is a return to the previous climate condition (Preto et al., 2010; Li et al., 2020). Furthermore, according to recent paleogeographic reconstructions (Golonka, 2004, 2007; Montenat, 2009; Muttoni et al., 2009a, 2009b; Zanchi et al., 2009a; Zanchi and Gaetani, 2011; Zanchetta et al., 2013; Angiolini et al., 2013, 2015; Zanchetta et al., 2018; Barrier et al., 2018), the Cimmerian continent of Şengör (1984) consisted in several different minor block which collided with the Laurasian margin in different times spanning from the Late Triassic up to the Early Jurassic. The collision of the Iran microplate with the Southern Eurasian margin (Nikishin et al., 1998; Muttoni et al., 2009a, b; Fürsich et al., 2009a; Zanchi et al., 2009a) had happened at an earlier time during the

Late Triassic between the end of Carnian and the Norian, while the other Cimmerian blocks collided later. In Afghanistan, the composite Band-e Bayan - Helmand Block (Farah Rud Block) are thought to collide with Eurasia between the Rhaetian and the middle Pliensbachian (Montenat, 2009; Siehl, 2017). Central Pamir collided with the Eurasian margin represented by the Karakul Mazar arc at around 200 Ma (Robinson, 2015), followed by Southern Pamir and Karakoram, whose progressive collisions occurred respectively at the end of the Triassic (Permian-Triassic boundary) and at the beginning of the Jurassic (Zanchi and Gaetani, 2011; Angiolini et al., 2013, 2015; Zanchetta et al., 2018). Finally, South Qiangtang is believed to have accreted to North Qiangtang at the end of the Triassic (Kapp et al., 2003; Zhai et al., 2011). Moreover, a sudden sharp rise in the Sr isotope records from the pelagic limestone succession of the Pizzo Mondello, Italy, at the beginning of the Lacian–Alaunian (lower-middle Norian) points to the rapid uplift and erosion of the Cimmerian orogen resulted from the accretion of the Iranian Cimmerian terranes to southern Laurasia at that time (Onoue et al., 2018). Chu et al. (2021) considered the timing of collision between Central Iran and Laurasia in NE Iran, as no later than 228 ± 3 Ma based on detrital zircon age spectra of the Triassic Mashad Phyllite (Binalud Mountains), which is so young respect to the CPE that dated through biostratigraphic calibration from Julian 2 to the Tuvalian 2 intervals (about 234–232 Ma: cf. Dal Corso et al., 2020; Colombi et al., 2021). However, the timing of collision initiation proposed by Chu et al. (2021) is in agreement with this study, pointing to the start of the collision after the CPE.

8. Conclusions

The Iran Plate as part of the Cimmerian terranes collided with the Turan Domain (southern margin of Laurasia) during the Late Triassic and gave origin to the Eo-Cimmerian Orogeny. The deformation of surrounding arc-related basins well records this compressional event, but the exact timing of this collision has long been debated. The Aghdarband Basin preserves a record of the Eo-Cimmerian orogenic event reflected in the severe deformation structures of its Triassic units. The Upper Triassic shale-dominated Miankuhi Formation of the Aghdarband Basin are the youngest rock units that convey the intense deformations they have endured, where strong folding, faulting, and deformational phases have been observed on these rocks.
In the present study, the Middle to Upper Triassic succession of the Aghdarband basin has been precisely analyzed through a multidisciplinary approach, and allowing us to review previous scenarios and to make new remarks on the evolution of the basin:

- Stratigraphy and sedimentology of the Aghdarband succession has been reviewed, and the transition from a deep marine environment to a delta setting and then an alluvial to marginal marine environment has been depicted. This interpretation led to redefining the depositional sequences and the meaning of the main erosional unconformity separating the Sina and Miankhui formations;
- Palynological and paleobotanical data collected from the Sina and Miankhui formations confirmed some points of the sedimentary evolution and overall allowed to refine the age of the succession. Particularly, the lower part of the Miankhui formation was deposited from the latest early Carnian to late Carnian age. Sufficient-resolution palynological data unravel the vegetation history of the studied formations: the vegetation pattern of the lower Miankhui formation, rich in hygrophytic elements, show clear evidence of a wet alluvial plain environment, supporting a strong correlation with the Carnian Pluvial Episode (CPE) and thus representing its only clear record in Iran region;
- The occurrence of a sea-level drop associated with a humid climate leading to high weathering rates can produce the significant unconformity at the base of the Miankhui formation, and the role of the eo-Cimmerian collision is revised, concerning the global impact and the short duration nature of the CPE and also the diachronous nature of Cimmerian collision in different structural blocks;
- Integrating results from the Aghdarband basin and data from the surrounding sedimentary basins, the onset of Eo-Cimmerian orogeny can be constrained to a period older than Middle Norian (217 ± 1.7 Ma) but younger than the late Carnian, at least in the case of the NE Iranian segment of the Paleotethys suture zone. Therefore, it is evident that the onset of CPE predates the Eo-Cimmerian collision, and the latter can be excluded as the primary cause of the "mid-Carnian" climatic perturbation.

Acknowledgments

This paper is dedicated to the memory of Prof. Ebrahim Ghasemi-Nejad, who contributed greatly to this paper. We thank the cooperation of colleagues from the Geological Survey of Iran, the Mashhad branch, particularly Jafar Taheri, Abradat Maafi, and Maryam Hosseiniyoon, and the University of Tehran for assistance in fieldwork. Thanks also to Mine Engineer Hajiyan (from Maadan Khavar) for providing hospitality at the Aghdarband Coal mine during our fieldwork. We thank Prof. M. Balini, Prof. G. Muttoni, Dr. A. Bertinelli, and

Dr. Dal Corso for their suggestions and discussions. M.M-J., M.C., and P.G. acknowledge Far 2018-2019 founding of the University of Ferrara.

References

Aghanabati, S.A., 2004. Geology of Iran. Geological Survey of Iran. 606 p. [in Persian]

Abedini, A., Mongelli, G., Khosravi, M., 2021. Geochemical constraints on the middle Triassic Kani Zarrineh karst bauxite deposit, Irano–Himalayan belt, NW Iran: Implications for elemental fractionation and parental affinity. Ore Geol. Rev. 133, 104099. https://doi.org/10.1016/J.OREGEOREV.2021.104099

Alavi, M., 1991. Sedimentary and structural characteristics of the Paleo-Tethys remnants in northeastern Iran. GSA Bulletin. 103.8, 983-992 https://pubs.geoscienceworld.org/gsa/gsabulletin/article/103/8/983/182620

Alavi, M., Vaziri, H., Seyed-Emami, K., Lasemi, Y., 1997. The Triassic and associated rocks of the Nakhlak and Aghdarband areas in central and northeastern Iran as remnants of the southern Turanian active continental margin. Bull. Geol. Soc. Am. 109, 1563–1575. https://doi.org/10.1130/0016-7606(1997)109<1563:TTAARO>2.3.CO;2

Allen, M., Jackson, J., Walker, R., 2004. Late Cenozoic reorganization of the Arabia-Eurasia collision and the comparison of short-term and long-term deformation rates. Tectonics 23. https://doi.org/10.1029/2003TC001530

Allen, M.B., Kheirkhah, M., Emami, M.H., Jones, S.J., 2011. Right-lateral shear across Iran and kinematic change in the Arabia-Eurasia collision zone. Geophys. J. Int. 184, 555–574. https://doi.org/10.1111/j.1365-246X.2010.04874.x

Angiolini, L., Crippa, G., Muttoni, G., Pignatti, J., 2013. Guadalupian (Middle Permian) paleobiogeography of the Neotethys Ocean. Gondwana Res. 24, 173–184. https://doi.org/10.1016/J.GR.2012.08.012

Angiolini, L., Zanchi, A., Zanchetta, S., Nicora, A., Vuolo, I., Berra, F., Henderson, C., Malaspina, N., Rettori, R., Vachard, D., Vezzoli, G., 2015. From rift to drift in South Pamir (Tajikistan): Permian evolution of a Cimmerian terrane. J. Asian Earth Sci. 102, 146–169.

https://doi.org/10.1016/J.JSEAES.2014.08.001

Arche, A., López-Gómez, J., 2014. The Carnian Pluvial Event in Western Europe: New data from Iberia and correlation with the Western Neotethys and Eastern North America-NW Africa regions. Earth-Science Rev. 128, 196–231. https://doi.org/10.1016/j.earscirev.2013.10.012

Balini, M., Nicora, A., Berra, F., Garzanti, E., Levera, M., Mattei, M., Muttoni, G., Zanchi, A., Bollati, I., Larghi, C., Zanchetta, S., Salamati, R., Mossavvari, F., 2009. The Triassic stratigraphic succession of Nakhlak (central Iran) a record from an active margin. Geol. Soc. Spec. Publ. 312, 287–321. https://doi.org/10.1144/SP312.14

Balini, M., Lucas, S.G., Jenks, J.F., Spielmann, J.A., 2010. Triassic ammonoid biostratigraphy: an overview. Geol. Soc. London, Spec. Publ. 334, 221–262. https://doi.org/10.1144/SP334.10

Balini, M., Nicora, A., Zanchetta, S., Zanchi, A., Marchesi, R., Vuolo, I., Hosseiniyoon, M., Norouzi, M., Soleimani, S., 2019. Olenekian to Early Ladinian stratigraphy of the western part of the Aghdarband window (Kopeh-Dagh, NE Iran), Rivista Italiana di Palaeontologia e Stratigrafia, 125(1), 283-315. https://doi.org/10.13130/2039-4942/11446

Balme, B.E., 1995. Fossil in situ spores and pollen grains: an annotated catalogue. Rev. Palaeobot. Palynol. 87, 81–323. https://doi.org/10.1016/0034-6667(95)93235-X

Baranyi, V., Miller, C.S., Ruffell, A., Hounslow, M.W., Kürschner, W.M., 2018. A continental record of the carnian pluvial episode (CPE) from the mercia mudstone group (UK): Palynology and climatic implications. J. Geol. Soc. London. 176, 149–166. https://doi.org/10.1144/jgs2017-150

Baranyi, V., Rostási, Á., Raucsik, B., Kürschner, W.M., 2019. Palynology and weathering proxies reveal climatic fluctuations during the Carnian Pluvial Episode (CPE) (Late Triassic) from marine successions in the Transdanubian Range (western Hungary). Glob. Planet. Change 177, 157–172. https://doi.org/10.1016/j.gloplacha.2019.01.018

Barrenechea, J.F., López-Gómez, J., Horra, R.D. La, 2018. Sedimentology, clay mineralogy and palaeosols of the Mid-Carnian Pluvial Episode in eastern Spain: insights into humidity and sea-level variations. J. Geol. Soc. London. 175, 993–1003. https://doi.org/10.1144/JGS2018-024

Barrier, E., Vrielynck, B., Brrouillet J.F., Brunet M.-F., 2018. Plaeotectonic reconstruction of the Central Tethyan Realm. Tectono-Sedimentary-Palinspastic maps from Late Permian to Pliocene. Commission for the Geological Map of the World (CGMW / CCGM), Paris, France.

Baud, Aymon, Brandner, R., Donofrio, D.A., 1991a. The Sefid Kuh Limestone-A late Lower Triassic Carbonate Ramp (Aghdarband, NE-Iran). triassic Aghdarband (AqDarband), NE-Iran, its pre-triassic Fram. 38, 111–123.

Baud, Aymon, Stampfli, G.M., Steen, D., 1991b. The Triassic Aghdarband Group: volcanism and geological evolution. Abhandlungen der Geol. Bundesanstalt 38, 125–137.

Berberian, M., King, G.C.P., 1981. Towards a paleogeography and tectonic evolution of Iran. Can. J. Earth Sci. 18, 210–265. https://doi.org/10.1139/e81-019

Bernardi, M., Gianolla, P., Petti, F.M., Mietto, P., Benton, M.J., 2018. Dinosaur diversification linked with the Carnian Pluvial Episode. Nat. Commun. 9. 1499. https://doi.org/10.1038/s41467-018-03996-1

Berner, U., Scheeder, G., Kus, J., Voigt, S., Schneider, J.W., 2009. Organic geochemical characterization of terrestrial source rocks of the Triassic Madygen Formation (Southern Tien Shan, Kyrgyzstan). Oil Gas 3, 135–139.

Besse, J., Torcq, F., Gallet, Y., Ricou, L.E., Krystyn, L., Saidi, A., 1998. Late Permian to Late Triassic palaeomagnetic data from Iran: constraints on the migration of the Iranian block through the Tethyan Ocean and initial destruction of Pangaea. Geophys. J. Int. 135, 77–92. https://doi.org/10.1046/J.1365-246X.1998.00603.X

Bittner, A., 1895. Lamellibranchiaten der Alpinen Trias. 1. Revision der Lamellibranchiaten von St. Cassian. Abh. Geol. Reichsanst. 18, 1–235.

Boersma, M., Van Konijnenburg-van Cittert, J.H.A., 1991. Late Triassic plant megafossils from Aghdarband (NE-Iran). Abhandlungen der Geol. Bundesanstalt 38, 223–252.

Boulin, J., 1988. Hercynian and Eocimmerian events in Afghanistan and adjoining regions. Tectonophysics 148, 253–278.

https://doi.org/10.1016/0040-1951(88)90134-5

Breda, A., Preto, N., Roghi, G., Furin, S., Meneguolo, R., Ragazzi, E., Fedele, P., Gianolla, P., others, 2009. The Carnian Pluvial Event in the Tofane area (Cortina d'Ampezzo, Dolomites, Italy). Geo. Alp 6, 80–115.

Bujak, J.P., Fisher, M.J., 1976. Dinoflagellate Cysts from the Upper Triassic of Arctic Canada. Micropaleontology 22, 44. https://doi.org/10.2307/1485320

Buryakovsky, L., Aminzadeh, F., Chilingarian, G. V, 2001. Petroleum geology of the south Caspian Basin. Elsevier.

Caggiati, M., Gianolla, P., Breda, A., Celarc, B., Preto, N., 2018. The start-up of the Dolomia Principale/Hauptdolomit carbonate platform (Upper Triassic) in the eastern Southern Alps. Sedimentology 65, 1097–1131. https://doi.org/10.1111/SED.12416

Calzolari, G., Rossetti, F., Seta, M. Della, Nozaem, R., Olivetti, V., Balestrieri, M.L., Cosentino, D., Faccenna, C., Stuart, F.M., Vignaroli, G., 2016. Spatio-temporal evolution of intraplate strike-slip faulting: The Neogene-Quaternary Kuh-e-Faghan Fault, central Iran. Bull. Geol. Soc. Am. 128, 374–396. https://doi.org/10.1130/B31266.1

Cao, W., Zahirovic, S., Flament, N., Williams, S., Golonka, J., Dietmar Müller, R., 2017. Improving global paleogeography since the late Paleozoic using paleobiology. Biogeosciences 14, 5425–5439. https://doi.org/10.5194/bg-14-5425-2017

Catuneanu, O., 2006. Principles of sequence stratigraphy. Elsevier. Amesterdam. 375 pp.

Chu, Y., Wan, B., Allen, M.B., Chen, L., Lin, W., Talebian, M., 2021. Tectonic evolution of Paleo-Tethys in NE Iran. EGUGA EGU21-3557.

Colombi, C., Martínez, R.N., Césari, S.N., Alcober, O., Limarino, C.O., Montañez, I., 2021. A high-precision U–Pb zircon age constraints the timing of the faunistic and palynofloristic events of the Carnian Ischigualasto Formation, San Juan, Argentina. J. South Am. Earth Sci. 111, 103433. https://doi.org/10.1016/J.JSAMES.2021.103433

Dal Corso, J., Mietto, P., Newton, R.J., Pancost, R.D., Preto, N., Roghi, G., Wignall, P.B., 2012. Discovery of a major negative δ13C spike in the Carnian (Late Triassic) linked to the eruption of Wrangellia flood basalts. Geology 40, 79–82. https://doi.org/10.1130/G32473.1

Dal Corso, J., Gianolla, P., Newton, R.J., Franceschi, M., Roghi, G., Caggiati, M., Raucsik, B., Budai, T., Haas, J., Preto, N., 2015. Carbon isotope records reveal synchronicity between carbon cycle perturbation and the "Carnian Pluvial Event" in the Tethys realm (Late Triassic). Glob. Planet. Change 127, 79–90. https://doi.org/10.1016/j.gloplacha.2015.01.013

Dal Corso, J., Gianolla, P., Rigo, M., Franceschi, M., Roghi, G., Mietto, P., Manfrin, S., Raucsik, B., Budai, T., Jenkyns, H.C., Reymond, C.E., Caggiati, M., Gattolin, G., Breda, A., Merico, A., Preto, N., 2018. Multiple negative carbon-isotope excursions during the Carnian Pluvial Episode (Late Triassic). Earth-Science Rev. https://doi.org/10.1016/j.earscirev.2018.07.004

Dal Corso, J., Bernardi, M., Sun, Y., Song, H., Seyfullah, L.J., Preto, N., Gianolla, P., Ruffell, A., Kustatscher, E., Roghi, G., Merico, A., Hohn, S., Schmidt, A.R., Marzoli, A., Newton, R.J., Wignall, P.B., Benton, M.J., 2020. Extinction and dawn of the modern world in the Carnian (Late Triassic). Sci. Adv. https://doi.org/10.1126/sciadv.aba0099

Davies, R.B., and Simmons, M.D., 2018. Triassic sequence stratigraphy of the Arabian Plate. Low. Triassic to Middle Jurassic Seq. Arab. Plate 101–162.

Davies, R. B., and Simmons, M.D., 2020. Dating and correlation of the Baluti Formation, Kurdistan, Iraq: Implications for the regional recognition of a Carnian "marker dolomite", and a review of the Triassic to Early Jurassic sequence stratigraphy of the Arabian Plate by G. A. Lunn, S. Miller and A. Samarrai. Discussion. Journal of Petroleum Geology, 43, 95-108. https://doi.org/10.1111/jpg.12751

Donofrio, D.A., 1991. Radiolaria and Porifera (spicula) from the Upper Triassic of Aghdarband (NE-Iran). Abhandlungen der Geol. Bundes-Anstalt 38, 205–222.

Eftekharnezhad, J., Behroozi, A., 1991. Geodynamic significance of recent discoveries of ophiolites and late Paleozoic rocks in NE-Iran (including Kopet Dagh). Abhandlungen der Geol. Bundesanstalt 38, 89–100.

Fijałkowska-Mader, A., 1999. Palynostratigraphy, palaeoecology and palaeoclimatology of the Triassic in South-Eastern Poland. Epic. Triassic 1, 601–627.

Fijałkowska-Mader, A., Jewuła, K., Bodor, E., 2021. Record of the Carnian Pluvial Episode in the Polish microflora. Palaeoworld 30, 106–125. https://doi.org/10.1016/J.PALWOR.2020.03.006

Franz, M., Nowak, K., Berner, U., Heunisch, C., Bandel, K., Röhling, H.G., Wolfgramm, M., 2014. Eustatic control on epicontinental basins: The example of the stuttgart formation in the central european basin (Middle Keuper, Late Triassic). Glob. Planet. Change 122, 305–329. https://doi.org/10.1016/j.gloplacha.2014.07.010

Franz, M., Kustatscher, E., Heunisch, C., Niegel, S., Röhling, H.-G., 2019. The Schilfsandstein and its flora; arguments for a humid mid-Carnian episode? J. Geol. Soc. London. 176, 133–148. https://doi.org/10.1144/JGS2018-05

Fu, X., Wang, J., Wen, H., Wang, Z., Zeng, S., Song, C., Chen, W., Wan, Y., 2020. A possible link between the Carnian Pluvial Event, global carbon-cycle perturbation, and volcanism: New data from the Qinghai-Tibet Plateau. Glob. Planet. Change 194, 103300. https://doi.org/10.1016/J.GLOPLACHA.2020.103300

Furin, S., Preto, N., Rigo, M., Roghi, G., Gianolla, P., Crowley, J.L., Bowring, S.A., 2006. High-precision U-Pb zircon age from the Triassic of Italy: Implications for the Triassic time scale and the Carnian origin of calcareous nannoplankton and dinosaurs. Geology 34, 1009–1012. https://doi.org/10.1130/G22967A.1

Fürsich, F.T., Hautmann, M., 2007. Bivalve reefs from the Upper Triassic of Iran. Museol. Sci. e Nat. 151, 13–23. https://doi.org/10.15160/1824-2707/351

Fürsich, F.T., Wilmsen, M., Seyed-Emami, K., Majidifard, M.R., 2009a. The Mid-Cimmerian tectonic event (Bajocian) in the Alborz Mountains, Northern Iran: evidence of the break-up unconformity of the South Caspian Basin. Geol. Soc. London, Spec. Publ. 312, 189–203. https://doi.org/10.1144/SP312.9

Fürsich, F.T., Wilmsen, M., Seyed-Emami, K., Majidifard, M.R., 2009b. Lithostratigraphy of the Upper Triassic–Middle Jurassic Shemshak Group of Northern Iran. Geol. Soc. London, Spec. Publ. 312, 129–160. https://doi.org/10.1144/SP312.6

Gaetani, M., 1997. The Nonh Karakoram in the framework of the Cimmerian blocks. Him. Geol 18, 33–48.

Garzanti, E., Gaetani, M., 2002. Unroofing history of Late Paleozoic magmatic arcs within the "Turan Plate" (Tuarkyr, Turkmenistan). Sediment. Geol. 151, 67–87. https://doi.org/10.1016/S0037-0738(01)00231-7

Gattolin, G., Preto, N., Breda, A., Franceschi, M., Isotton, M., Gianolla, P., 2015. Sequence stratigraphy after the demise of a high-relief carbonate platform (Carnian of the Dolomites): Sea-level and climate disentangled. Palaeogeogr. Palaeoclimatol. Palaeoecol. 423, 1–17.

Ghasemi-Nejad, E., Head, M.J., Zamani, M., 2008. Dinoflagellate cysts from the Upper Triassic (Norian) of northeastern Iran. J. Micropalaeontology 27, 125–134. https://doi.org/10.1144/JM.27.2.125

Gianolla, P., Jacquin, T., 1998. Triassic Sequence Stratigraphic Framework of Western European Basins. In: de Graciansky, P.-C., Hardenbol, J., Jacquin, T., Vail, P.R. (Eds.), Mesozoic and Cenozoic Sequence Stratigraphy of European Basins. SEPM Special Publications, 643–650. https://doi.org/10.2110/pec.98.02.0643

Gianolla, P., De Zanche, V., Mietto, P., 1998. Triassic sequence stratigraphy in the Southern Alps (northern Italy): definition of sequences and basin evolution. In: de Graciansky, P.-C., Hardenbol, J., Jacquin, T., Vail, P.R. (Eds.), Mesozoic and Cenozoic Sequence Stratigraphy of European Basins. SEPM Special Publications, 719–747. https://doi.org/10.2110/pec.98.02.0719.

Gianolla, P., Caggiati, M., Riva, A., 2021. The interplay of carbonate systems and volcanics: Cues from the 3D model of the Middle Triassic Sciliar/Schlern platform (Dolomites, Southern Alps). Mar. Pet. Geol. 124, 104794. https://doi.org/10.1016/J.Marpetgeo.2020.104794

Golonka, J., 2004. Plate tectonic evolution of the southern margin of Eurasia in the Mesozoic and Cenozoic. Tectonophysics 381, 235–273.

https://doi.org/10.1016/J.TECTO.2002.06.004

Golonka, J., 2007. Late Triassic and Early Jurassic palaeogeography of the world. Palaeogeogr. Palaeoclimatol. Palaeoecol. 244, 297–307. https://doi.org/10.1016/J.PALAEO.2006.06.041

Hagdorn, H., Wang, X., Wang, C., 2007. Palaeoecology of the pseudoplanktonic Triassic crinoid Traumatocrinus from Southwest China. Palaeogeogr. Palaeoclimatol. Palaeoecol. 247, 181–196. https://doi.org/10.1016/J.PALAEO.2006.10.020

Hanna, M.T., 2007. Palynology of the upper part of the Baluti formation (Upper Triassic) and the nature of its contact with the Sarki formation at Amadiya district, northern Iraq. Ph. D Thesis, University of Mosul, Iraq.

Haq, B.U., 2018. Triassic eustatic variations reexamined. GSA Today 28, 4–9. https://doi.org/10.1130/GSATG381A.1

Hardenbol, J., Thierry, J., Farley, M.B., Jacquin, T., de Graciansky, P.C., Vail, P.R., 1998, cs. In: P.C. de Graciansky, J. Hardenbol, T. Jacquin, P.R. Vail and D. Ulmer-Scholle (Eds.): Mesozoic and Cenozoic sequence stratigraphy of European basins: SEPM Special Publication, 60, 3–13. https://doi.org/10.2110/pec.98.02.0003

Hochuli, P.A., Frank, S.M., 2000. Palynology (dinoflagellate cysts, spore-pollen) and stratigraphy of the Lower Carnian Raibl Group in the Eastern Swiss Alps. Eclogae Geol. Helv. 93, 429–444.

Hornung, T., Krystyn, L., Brandner, R., 2007. A Tethys-wide mid-Carnian (Upper Triassic) carbonate productivity crisis: Evidence for the Alpine Reingraben Event from Spiti (Indian Himalaya)? J. Asian Earth Sci. 30, 285–302. https://doi.org/10.1016/j.jseaes.2006.10.001

Horton, B.K., Hassanzadeh, J., Stockli, D.F., Axen, G.J., Gillis, R.J., Guest, B., Amini, A., Fakhari, M.D., Zamanzadeh, S.M., Grove, M., 2008. Detrital zircon provenance of Neoproterozoic to Cenozoic deposits in Iran: Implications for chronostratigraphy and collisional tectonics. Tectonophysics 451, 97–122. https://doi.org/10.1016/J.TECTO.2007.11.063

Jelen, B., 1982. Quantitative palynologîcal analysis of Julian clastic rocks from the lead-zinc deposit of Mežica. Geologija 25(2), 213-227.

Jin, X., Gianolla, P., Shi, Z., Franceschi, M., Caggiati, M., Du, Y., Preto, N., 2020. Synchronized changes in shallow water carbonate production during the Carnian Pluvial Episode (Late Triassic) throughout Tethys. Glob. Planet. Change 184, 103035. https://doi.org/10.1016/j.gloplacha.2019.103035

Kapp, P., Murphy, M.A., Yin, A., Harrison, T.M., Ding, L., Guo, J., 2003. Mesozoic and Cenozoic tectonic evolution of the Shiquanhe area of western Tibet. Tectonics 22 (4), 1-23. https://doi.org/10.1029/2001TC001332

Kavary, E., 1966. A palynological study of the subdivision of the Cardita Shales (Upper Triassic) of Bleiberg, Austria. Verhandlungen der Geol. Bundesanstalt 1, 178–189.

Kazmin, V.G., 1990. Early Mesozoic reconstruction of the Black Sea-Caucasus region. Evol. North. margin Tethys. Mémo la Soc Géol Fr. Nouv. Ser 54, 147–158.

Kazmin, V.G., 1997. Mesozoic to Cenozoic history of the back-arc basins in the Black Sea-Caucasus region. CASP Rep., No. 656.

Klausen, T.G., Paterson, N.W., Benton, M.J., 2020. Geological control on dinosaurs' rise to dominance: Late Triassic ecosystem stress by relative sea level change. Terra Nov. 32, 434–441. https://doi.org/10.1111/TER.12480

Kozur, H.W., Bachmann, G.H., 2010. The Middle Carnian Wet Intermezzo of the Stuttgart Formation (Schilfsandstein), Germanic Basin. Palaeogeogr. Palaeoclimatol. Palaeoecol. 290, 107–119. https://doi.org/10.1016/j.palaeo.2009.11.004

Kräusel, R., Schaarschmidt, F., 1966. Die Keuperflora von Neuewelt bei Basel. IV. Pterophyllen und Taeniopteriden. Schweizer Paläontologische Abhandlungen 84, 3–44.

Kristan-Tollmann, E., Haas, J., Kovács, S., 1991. Karnische Ostracoden und Conodonten der Bohrung Zsámbék-14 im Transdanubischen Mittelgebirge (Ungarn), in: Jubiläumsschrift 20 Jahre Geologische Zusammenarbeit Osterreich-Ungarn; Wien-Bécs; 1991. pp. 193–219.

Krystyn, L., Tatzreiter, F., 1991. Middle Triassic ammonoids from Aghdarband (NE-Iran) and their paleobiogeographical significance. Abhandlungen der Geol. Bundesanstalt 38, 139–165.

Krystyn, L., Balini, M., Aghababalou, B.S., Hairapetian, V., 2019. Norian ammonoids from the nayband formation (Iran) and their bearing on late triassic sedimentary and geodynamic history of the Iran plate. Riv. Ital. di Paleontol. e Stratigr. 125, 231–248. https://doi.org/10.13130/2039-4942/11412

Kustatscher, E., Ash, S.R., Karasev, E., Pott, C., Vajda, V., Yu, J., McLoughlin, S., 2018. Flora of the Late Triassic. Springer, Cham, pp. 545–622. https://doi.org/10.1007/978-3-319-68009-5_13

Lehrmann, D.J., Enos, P., Payne, J.L., Montgomery, P., Wei, J., Yu, Y., Xiao, J., Orchard, M.J., 2005. Permian and Triassic depositional history of the Yangtze platform and Great Bank of Guizhou in the Nanpanjiang basin of Guizhou and Guangxi, south China. Albertiana 33, 149–168.

Li, Z., Chen, Z.Q., Zhang, F., Ogg, J.G., Zhao, L., 2020. Global carbon cycle perturbations triggered by volatile volcanism and ecosystem responses during the Carnian Pluvial Episode (late Triassic). Earth-Science Rev. 211, 103404. https://doi.org/10.1016/J.EARSCIREV.2020.103404

Liaghat, M., Adabi, M.H., Swennen, R., Mohammadi, Z., Alijani, H., 2021. An integrated facies, diagenesis and geochemical analysis along with sequence stratigraphy of the Lower Triassic Aghe-Darband basin (north-east Iran). J. African Earth Sci. 173, 103952. https://doi.org/10.1016/J.JAFREARSCI.2020.103952

Lunn, G.A., 2020. Dating and correlation of the baluti Formation, kurdistan, Iraq: Implications for the regional recognition of a Carnian “marker dolomite”, and a review of the Triassic to Early Jurassic sequence stratigraphy of the Arabian Plate. J. Pet. Geol. 43, 109–125.

https://doi.org/10.1111/JPG.12752

Lunn, G. A., Miller, S., Samarrai, A., 2019. Dating and correlation of the Baluti Formation, Kurdistan, Iraq: Implications for the regional recognition of a Carnian “marker dolomite”, and a review of the Triassic to Early Jurassic sequence stratigraphy of the Arabian Plate. J. Pet. Geol. 42, 5–36. https://doi.org/10.1111/JPG.12722

Mangerud, G., Paterson, N.W., Riding, J.B., 2019. The temporal and spatial distribution of Triassic dinoflagellate cysts. Rev. Palaeobot. Palynol. 261, 53–66. https://doi.org/10.1016/J.REVPALBO.2018.11.010

Mantle, D.J., Riding, J.B., Hannaford, C., 2020. Late Triassic dinoflagellate cysts from the Northern Carnarvon Basin, Western Australia. Rev. Palaeobot. Palynol. 281, 104254. https://doi.org/10.1016/J.REVPALBO.2020.104254

Mattei, M., Muttoni, G., Cifelli, F., 2014. A record of the Jurassic massive plate shift from the Garedu Formation of central Iran. Geology 42, 555–558. https://doi.org/10.1130/G35467.1

Mattei, M., Cifelli, F., Muttoni, G., Rashid, H., 2015. Post-Cimmerian (Jurassic–Cenozoic) paleogeography and vertical axis tectonic rotations of Central Iran and the Alborz Mountains. J. Asian Earth Sci. 102, 92–101. https://doi.org/10.1016/J.JSEAES.2014.09.038

Matthews, K.J., Maloney, K.T., Zahirovic, S., Williams, S.E., Seton, M., Müller, R.D., 2016. Global plate boundary evolution and kinematics since the late Paleozoic. Glob. Planet. Change 146, 226–250.

https://doi.org/10.1016/j.gloplacha.2016.10.002

Mazaheri-Johari, M., Kustatscher, E., Roghi, G., Ghasemi-Nejad, E., Gianolla, P., 2021. A monotypic stand of Neocalamites iranensis n. sp. from the Carnian Pluvial Episode (Late Triassic) of the Aghdarband area, NE Iran (Turan Plate). Riv. Ital. di Paleontol. e Stratigr. 127(2), 189-209.

Mazaheri-Johari, M., Gianolla, P., Mather, T.A., Frieling, J., Chu, D., Dal Corso, J., 2021. Mercury deposition in Western Tethys during the Carnian Pluvial Episode (Late Triassic). Sci. Rep. 11, 1–10. https://doi.org/10.1038/s41598-021-96890-8

Mietto, P., Manfrin, S., Preto, N., Rigo, M., Roghi, G., Furin, S., Gianolla, P., Posenato, R., Muttoni, G., Nicora, A., Buratti, N., Cirilli, S., Spötl, C., Ramezani, J., Bowring, S.A., Di, P., Stuores, S./, Section, W., Alps, S., Italy, N.E., 2012. The Global Boundary Stratotype Section and Point (GSSP) of the Carnian Stage (Late Triassic). Episodes 35, 414–430.

https://doi.org/10.18814/epiiugs/2012/v35i3/003.

Mietto, P., Avanzini, M., Belvedere, M., Bernardi, M., Vecchia, F.M.D., Porchetti, S.D., Gianolla, P., Petti, F.M., 2020. Triassic tetrapod ichnofossils from Italy: the state of the art. J. Mediterr. Earth Sci. 12, 83–136.

https://doi.org/10.3304/JMES.2020.17066

Miller, C.S., Peterse, F., da Silva, A.-C., Baranyi, V., Reichart, G.J., Kürschner, W.M., 2017. Astronomical age constraints and extinction mechanisms of the Late Triassic Carnian crisis. Sci. Reports 2017 71 7, 1–7. https://doi.org/10.1038/s41598-017-02817-7

Mirnejad, H., Lalonde, A.E., Obeid, M., Hassanzadeh, J., 2013. Geochemistry and petrogenesis of Mashhad granitoids: An insight into the geodynamic history of the Paleo-Tethys in northeast of Iran. Lithos 170–171, 105–116. https://doi.org/10.1016/J.LITHOS.2013.03.003

Moisan, P., Voigt, S., Schneider, J.W., Kerp, H., 2012. New fossil bryophytes from the Triassic Madygen Lagerstätte (SW Kyrgyzstan). Rev. Palaeobot. Palynol. 187, 29–37. https://doi.org/10.1016/j.revpalbo.2012.08.009

Moisan, P., Krings, M., Voigt, S., Kerp, H., 2021. Fossil roots with root nodules from the Madygen Formation (Ladinian–Carnian; Triassic) of Kyrgyzstan. Geobios 64, 65–75. https://doi.org/10.1016/J.GEOBIOS.2020.10.004

Montenat, C., 2009. The Mesozoic of Afghanistan. GeoArabia 14, 147–210.

Morley, C.K., Kongwung, B., Julapour, A.A., Abdolghafourian, M., Hajian, M., Waples, D., Warren, J., Otterdoom, H., Srisuriyon, K., Kazemi, H., 2009. Structural development of a major late Cenozoic basin and transpressional belt in central Iran: The Central Basin in the Qom-Saveh areaCenozoic transpression Central Iran. Geosphere 5, 325–362. https://doi.org/10.1130/GES00223.1

Mueller, S., Hounslow, M.W., Kürschner, W.M., 2016a. Integrated stratigraphy and palaeoclimate history of the Carnian Pluvial Event in the Boreal realm; new data from the Upper Triassic Kapp Toscana Group in central Spitsbergen (Norway). J. Geol. Soc. London 173, 186–202. https://doi.org/doi:10.1144/jgs2015-028

Mueller, S., Krystyn, L., Kürschner, W.M., 2016b. Climate variability during the Carnian Pluvial Phase — A quantitative palynological study of the Carnian sedimentary succession at Lunz am See, Northern Calcareous Alps, Austria. Palaeogeogr. Palaeoclimatol. Palaeoecol. 441, 198–211. https://doi.org/10.1016/J.PALAEO.2015.06.008

Muttoni, G., Mattei, M., Balini, M., Zanchi, A., Gaetani, M., Berra, F., 2009a. The drift history of Iran from the Ordovician to the Triassic. Geol. Soc. London, Spec. Publ. 312, 7–29. https://doi.org/10.1144/SP312.2

Muttoni, G., Gaetani, M., Kent, D. V., Sciunnach, D., Angiolini, L., Berra, F., Garzanti, E., Mattei, M., Zanchi, A., 2009b. Opening of the Neo-tethys ocean and the pangea B to pangea A transformation during the permian. GeoArabia 14, 17–48.

Muttoni, G., Tartarotti, P., Chiari, M., Marieni, C., Rodelli, D., Dallanave, E., Kirscher, U., 2015. Paleolatitudes of Late Triassic radiolarian cherts from Argolis, Greece: Insights on the paleogeography of the western Tethys. Palaeogeogr. Palaeoclimatol. Palaeoecol. 417, 476–490. https://doi.org/10.1016/j.palaeo.2014.10.010

Natal'in, B.A., Şengör, A.M.C., 2005. Late Palaeozoic to Triassic evolution of the Turan and Scythian platforms: The pre-history of the Palaeo-Tethyan closure. Tectonophysics 404, 175–202. https://doi.org/10.1016/J.TECTO.2005.04.011

Nikishin, A.M., Cloetingh, S., Brunet, M.-F., Stephenson, R.A., Bolotov, S.N., Ershov, A. V, 1998. Scythian platform, Caucasus and Black Sea region: Mesozoic--Cenozoic tectonic history and dynamics. Peri-Tethys Mem. 3, 163–176.

Nozaem, R., Mohajjel, M., Rossetti, F., Della Seta, M., Vignaroli, G., Yassaghi, A., Salvini, F., Eliassi, M., 2013. Post-Neogene right-lateral strike-slip tectonics at the north-western edge of the Lut Block (Kuh-e-Sarhangi Fault), Central Iran. Tectonophysics 589, 220–233. https://doi.org/10.1016/j.tecto.2013.01.001

Ogg, J.G., Chen, Z.-Q., Orchard, M.J., Jiang, H.S., 2020. The Triassic Period, Geologic Time Scale 2020. Elsevier. 903-953 https://doi.org/10.1016/b978-0-12-824360-2.00025-5

Onoue, T., Yamashita, K., Fukuda, C., Soda, K., Tomimatsu, Y., Abate, B., Rigo, M., 2018. Sr isotope variations in the Upper Triassic succession at Pizzo Mondello, Sicily: Constraints on the timing of the Cimmerian Orogeny. Palaeogeogr. Palaeoclimatol. Palaeoecol. 499, 131–137. https://doi.org/10.1016/J.PALAEO.2018.03.025

Praehauser-Enzenberg, M., 1970. Beitrag zur mikroflora der obertrias von Heiligkreuz (Gadertal, Dolomiten). Festband Geol. Inst 321–337.

Preto, N., Kustatscher, E., Wignall, P.B., 2010. Triassic climates - State of the art and perspectives. Palaeogeogr. Palaeoclimatol. Palaeoecol. 290, 1–10. https://doi.org/10.1016/j.palaeo.2010.03.015

Riding, J.B., Mantle, D.J., Backhouse, J., 2010. A review of the chronostratigraphical ages of Middle Triassic to Late Jurassic dinoflagellate cyst biozones of the North West Shelf of Australia. Rev. Palaeobot. Palynol. 162, 543–575. https://doi.org/10.1016/J.REVPALBO.2010.07.008

Robert, A.M.M., Letouzey, J., Kavoosi, M.A., Sherkati, S., Müller, C., Vergés, J., Aghababaei, A., 2014. Structural evolution of the Kopeh Dagh fold-and-thrust belt (NE Iran) and interactions with the South Caspian Sea Basin and Amu Darya Basin. Mar. Pet. Geol. 57, 68–87. https://doi.org/10.1016/j.marpetgeo.2014.05.002

Robinson, A.C., 2015. Mesozoic tectonics of the Gondwanan terranes of the Pamir plateau. J. Asian Earth Sci. 102, 170–179. https://doi.org/10.1016/J.JSEAES.2014.09.012

Robinson, A.C., Ducea, M., Lapen, T.J., 2012. Detrital zircon and isotopic constraints on the crustal architecture and tectonic evolution of the northeastern Pamir. Tectonics 31. https://doi.org/10.1029/2011TC003013

Roghi, G., 2004. Palynological investigations in the Carnian of the Cave del Predil area (Julian Alps, NE Italy). Rev. Palaeobot. Palynol. 132, 1–35. https://doi.org/10.1016/J.REVPALBO.2004.03.001

Roghi, G., 2004. Palynological investigations in the Carnian of the Cave del Predil area (Julian Alps, NE Italy). Rev. Palaeobot. Palynol. 132, 1–35. https://doi.org/10.1016/J.REVPALBO.2004.03.001

Roghi, G., Gianolla, P., Minarelli, L., Pilati, C., Preto, N., 2010. Palynological correlation of Carnian humid pulses throughout western Tethys. Palaeogeogr. Palaeoclimatol. Palaeoecol. 290, 89–106. https://doi.org/10.1016/J.PALAEO.2009.11.006

Ruffell, A., Simms, M.J., Wignall, P.B., 2016. The Carnian Humid Episode of the late Triassic: A review. Geol. Mag. 153, 271–284.

https://doi.org/10.1017/S0016756815000424

Ruttner, A.W., 1991. The Triassic of Aghdarband (AqDarband), NE-lran, and its Pre-Triassic Frame Geology of the Aghdarband Area (Kopet Dagh, NE-lran). Abhandlungen der Geol. Bundes-Anstalt 38, 7–79.

Ruttner, A.W., 1993. Southern borderland of Triassic Laurasia in north-east Iran. Geol. Rundschau 1993 821 82, 110–120. https://doi.org/10.1007/BF00563274

Saidi, A., Brunet, M.-F., Ricou, L.-E., 2015. Continental accretion of the Iran Block to Eurasia as seen from Late Paleozoic to Early Cretaceous subsidence curves. http://dx.doi.org/10.1080/09853111.1997.11105302 10, 189–208. https://doi.org/10.1080/09853111.1997.11105302

Sengör, A.M.C., 1979. Mid-Mesozoic closure of Permo--Triassic Tethys and its implications. Nature 279, 590–593.

Şengör, A.M.C., 1990. A new model for the late Palaeozoic-Mesozoic tectonic evolution of Iran and implications for Oman. Geol. Soc. Spec. Publ. 49, 797–831. https://doi.org/10.1144/GSL.SP.1992.049.01.49

Şengör, A.M.C., 1984. The Cimmeride orogenic system and the tectonics of Eurasia. Geol. Soc. Am. Spec. Pap. 195, 82.

Seyed-Emami, K., 2003. Triassic in Iran. Facies 48, 91–106.

Seyed-Emami, K., Wilmsen, M., Fürsich, F., 2021. A summary of the Jurassic System in North and East-Central Iran, Zitteliana 94, 99-156.

Sheikholeslami, M.R., Kouhpeyma, M., 2012. Structural analysis and tectonic evolution of the eastern Binalud Mountains, NE Iran. J. Geodyn. 61, 23–46. https://doi.org/10.1016/j.jog.2012.06.010

Shi, Z., Preto, N., Jiang, H., Krystyn, L., Zhang, Y., Ogg, J.G., Jin, X., Yuan, J., Yang, X., Du, Y., 2017. Demise of Late Triassic sponge mounds along the northwestern margin of the Yangtze Block, South China: Related to the Carnian Pluvial Phase? Palaeogeogr. Palaeoclimatol. Palaeoecol. 474, 247–263. https://doi.org/10.1016/J.PALAEO.2016.10.031

Siblik, M., 1991. The Triassic of Aghdarband (AqDarband), NE-lran, and its Pre-Triassic Frame Triassic Brachiopods from Aghdarband (NE-lran). Abhandlungen der Geol.

Bundes-Anstalt 38, 165–174.

Siehl, A., 2017. Structural setting and evolution of the Afghan orogenic segment – a review. From: Brunet, M.-F., McCann, T. & Sobel, E. R. (eds) 2017. Geological Evolution of Central Asian Basins and the Western Tien Shan Range. Geological Society, London, Special Publications, 427, 57–88. https://doi.org/10.1144/SP427.8

Simms, M.J., Ruffell, A.H., 1989. Synchroneity of climatic change and extinctions in the Late Triassic. Geology 17, 265–268.

Stampfli, G.M., Borel, G.D., 2002. A plate tectonic model for the Paleozoic and Mesozoic constrained by dynamic plate boundaries and restored synthetic oceanic isochrons. Earth Planet. Sci. Lett. 196, 17–33. https://doi.org/10.1016/S0012-821X(01)00588-X

Stefani, M., Furin, S., Gianolla, P., 2010. The changing climate framework and depositional dynamics of Triassic carbonate platforms from the Dolomites. Palaeogeogr. Palaeoclimatol. Palaeoecol. 290, 43–57. https://doi.org/10.1016/j.palaeo.2010.02.018

Stöcklin, J., 1974. Possible Ancient Continental Margins in Iran. Geol. Cont. Margins 873–887. https://doi.org/10.1007/978-3-662-01141-6_64

Stocklin, J., Nabavi, M.H., 1973. Tectonic map of Iran. Geol. Surv. Iran 1, 5.

Sun, Y.D., Wignall, P.B., Joachimski, M.M., Bond, D.P.G., Grasby, S.E., Lai, X.L., Wang, L.N., Zhang, Z.T., Sun, S., 2016. Climate warming, euxinia and carbon isotope perturbations during the Carnian (Triassic) Crisis in South China. Earth Planet. Sci. Lett. 444, 88–100. https://doi.org/10.1016/j.epsl.2016.03.037

Taheri, J., Fürsich, F.T., Wilmsen, M., 2009. Stratigraphy, depositional environments and geodynamic significance of the Upper Bajocian–Bathonian Kashafrud Formation, NE Iran. Geol. Soc. London, Spec. Publ. 312, 205–218. https://doi.org/10.1144/SP312.10

Tamar-Agha, M.Y., Hakeem, F.A., Aqrawi, A.M., 2020. The sedimentology and paleoclimatology of Early Triassic regional marine oxic event (Beduh Formation), Kurdistan region – Northern Iraq. J. African Earth Sci. 163, 103742.

https://doi.org/10.1016/J.JAFREARSCI.2019.103742

Tomimatsu, Y., Nozaki, T., Sato, H., Takaya, Y., Kimura, J.I., Chang, Q., Naraoka, H., Rigo, M., Onoue, T., 2021. Marine osmium isotope record during the Carnian “pluvial episode” (Late Triassic) in the pelagic Panthalassa Ocean. Glob. Planet. Change 197, 103387. https://doi.org/10.1016/j.gloplacha.2020.103387

Torshizian, H.A., 2016. A study of the tectonic origin and the source of the clastic sediments of the Miankuhi formation in the Tarik Dareh region (Torbat Jam, NE Iran). Iranian Journal of Earth Sciences, 8, 45-51.

Van der Eem, J.G.L.A., 1983. Aspects of middle and late triassic palynology. 6. Palynological investigations in the Ladinian and lower Karnian of the Western Dolomites, Italy. Rev. Palaeobot. Palynol. 39, 189–300. https://doi.org/10.1016/0034-6667(83)90016-7

Vigran, J. O., Mangerud, G., Mørk, A., Worsley, D., & Hochuli, P. A. (2014). Palynology and geology of the Triassic succession of Svalbard and the Barents Sea. Norges geologiske undersokelse 14, 270pp. http://www.ngu.no/no/

Visscher, H., van der Zwan, C.J., 1981. Palynology of the circum-mediterranean triassic: Phytogeographical and palaeoclimatological implications. Geol. Rundschau. 702 70, 625–634. https://doi.org/10.1007/BF01822140

Visscher, H., Van Houte, M., Brugman, W.A., Poort, R.J., 1994. Rejection of a Carnian (Late triassic) “pluvial event” in Europe. Rev. Palaeobot. Palynol. 83, 217–226. https://doi.org/10.1016/0034-6667(94)90070-1

Wiggins, V.D., 1973. Upper Triassic dinoflagellates from arctic Alaska. Micropaleontology 19, 1–16.

Wilmsen, M., Fürsich, F.T., Seyed-Emami, K., Majidifard, M.R., Taheri, J., 2009a. The Cimmerian Orogeny in northern Iran: tectono-stratigraphic evidence from the foreland. Terra Nov. 21, 211–218. https://doi.org/10.1111/J.1365-3121.2009.00876.X

Wilmsen, M., Fürsich, F.T., Taheri, J., 2009b. The Shemshak Group (Lower–Middle Jurassic) of the Binalud Mountains, NE Iran: stratigraphy, depositional environments and geodynamic implications. Geol. Soc. London, Spec. Publ. 312, 175–188. https://doi.org/10.1144/SP312.8

Wohrmann, F., S., 1889. Die Fauna der sogenannten Cardita-und Raibler-Schichten in den nordtiroler und bayrischen Alpen. Jahrb. der Kais. Geol. Reichsanstalt 39, 181–260.

Xu, G., Hannah, J.L., Stein, H.J., Mørk, A., Vigran, J.O., Bingen, B., Schutt, D.L., Lundschien, B.A., 2014. Cause of Upper Triassic climate crisis revealed by Re-Os geochemistry of Boreal black shales. Palaeogeogr. Palaeoclimatol. Palaeoecol. 395, 222–232. https://doi.org/10.1016/j.palaeo.2013.12.027

Zanchetta, S., Berra, F., Zanchi, A., Bergomi, M., Caridroit, M., Nicora, A., Heidarzadeh, G., 2013. The record of the Late Palaeozoic active margin of the Palaeotethys in NE Iran: Constraints on the Cimmerian orogeny. Gondwana Res. 24, 1237–1266. https://doi.org/10.1016/J.GR.2013.02.013

Zanchetta, S., Worthington, J., Angiolini, L., Leven, E.J., Villa, I.M., Zanchi, A., 2018. The Bashgumbaz Complex (Tajikistan): Arc obduction in the Cimmerian orogeny of the Pamir. Gondwana Res. 57, 170–190. https://doi.org/10.1016/J.GR.2018.01.009

Zanchi, A., Gaetani, M., 2011. The geology of the Karakoram range, Pakistan: the new 1:100,000 geological map of Central-Western Karakoram. Ital. J. Geosci. 130, 161–262. https://doi.org/10.3301/IJG.2011.09

Zanchi, A., Zanchetta, S., Berra, F., Mattei, M., Garzanti, E., Molyneux, S., Nawab, A., Sabouri, J., 2009a. The Eo-Cimmerian (Late? Triassic) orogeny in North Iran. Geol. Soc. London, Spec. Publ. 312, 31–55. https://doi.org/10.1144/SP312.3

Zanchi, A., Zanchetta, S., Garzanti, E., Balini, M., Berra, F., Mattei, M., Muttoni, G., 2009b. The Cimmerian evolution of the Nakhlak-Anarak area Central Iran and its bearing for the reconstruction of the historyof the Eurasian margin. Geol. Soc. Spec. Publ. 312, 261–286. https://doi.org/10.1144/SP312.13

Zanchi, A., Zanchetta, S., Balini, M., Ghassemi, M.R., 2016. Oblique convergence during the Cimmerian collision: Evidence from the Triassic Aghdarband Basin, NE Iran. Gondwana Res. 38, 149–170.

https://doi.org/10.1016/J.GR.2015.11.008

Zhai, Q.G., Jahn, B.M., Zhang, R.Y., Wang, J., Su, L., 2011. Triassic Subduction of the Paleo-Tethys in northern Tibet, China: Evidence from the geochemical and isotopic characteristics of eclogites and blueschists of the Qiangtang Block. J. Asian Earth Sci. 42, 1356–1370. https://doi.org/10.1016/J.JSEAES.2011.07.023

Zhang, Y., Li, M., Ogg, J.G., Montgomery, P., Huang, C., Chen, Z.Q., Shi, Z., Enos, P., Lehrmann, D.J., 2015. Cycle-calibrated magnetostratigraphy of middle Carnian from South China: Implications for Late Triassic time scale and termination of the Yangtze Platform. Palaeogeogr. Palaeoclimatol. Palaeoecol. 436, 135–166. https://doi.org/10.1016/J.PALAEO.2015.05.033

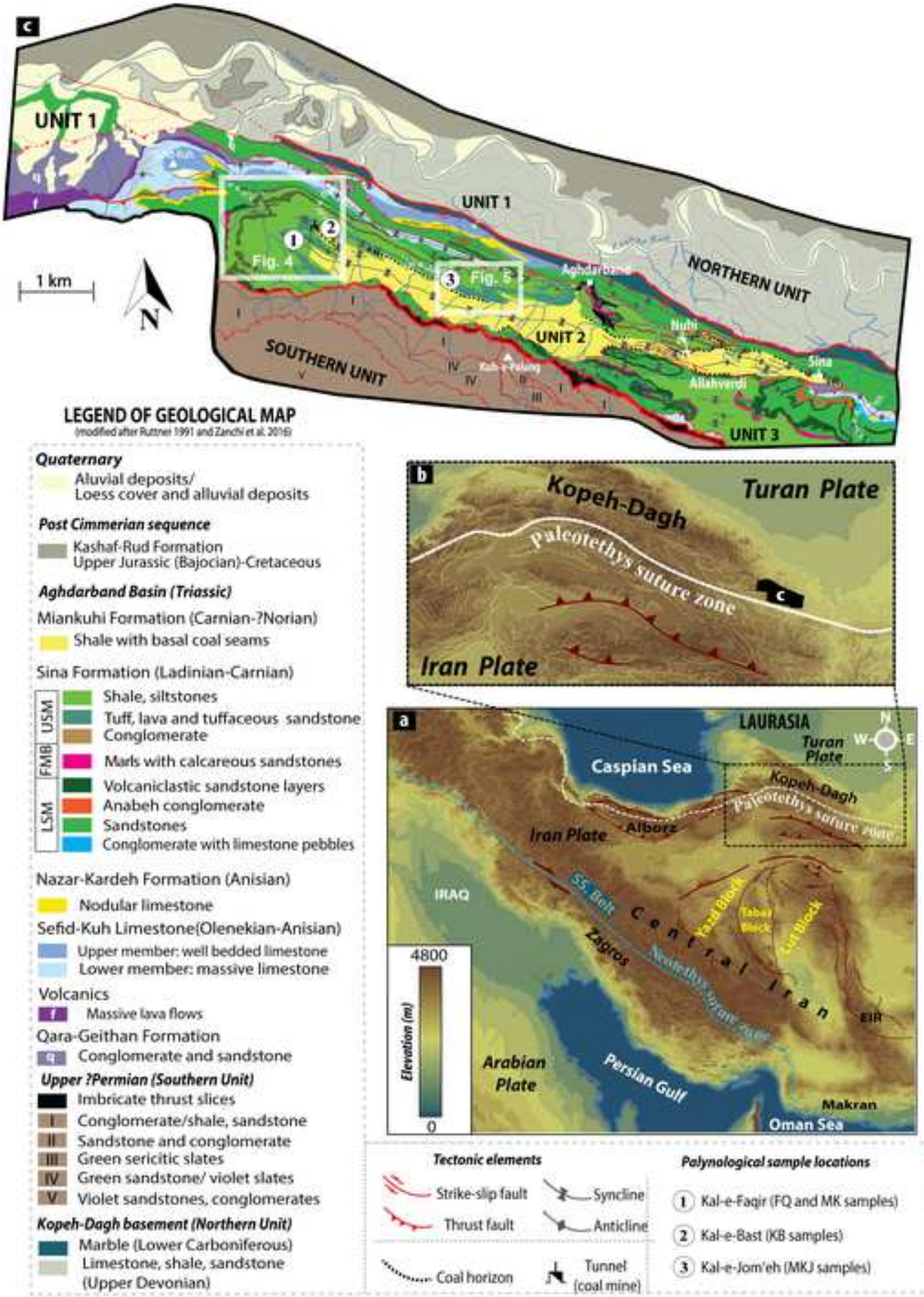
c
UNIT 1
UNIT 1
NORTHERN UNIT
UNIT 2
UNIT 3
SOUTHERN UNIT
Fig. 4
Fig. 5
Aghdarband
Nuhi
Sina
Allahverdi
Kuh-e-Palang
1 km
N
LEGEND OF GEOLOGICAL MAP
(modified after Ruttner 1991 and Zanchi et al. 2016)
Quaternary
Aluvial deposits/
Loess cover and alluvial deposits
Post Cimmerian sequence
Kashaf-Rud Formation
Upper Jurassic (Bajocian)-Cretaceous
Aghdarband Basin (Triassic)
Miankuhi Formation (Carnian-?Norian)
Shale with basal coal seams
Sina Formation (Ladinian-Carnian)
USM
FMB
LSM
Shale, siltstones
Tuff, lava and tuffaceous sandstone
Conglomerate
Marls with calcareous sandstones
Volcaniclastic sandstone layers
Anabeh conglomerate
Sandstones
Conglomerate with limestone pebbles
Nazar-Kardeh Formation (Anisian)
Nodular limestone
Sefid-Kuh Limestone(Olenekian-Anisian)
Upper member: well bedded limestone
Lower member: massive limestone
Volcanics
Massive lava flows
Qara-Geithan Formation
Conglomerate and sandstone
Upper ?Permian (Southern Unit)
Imbricate thrust slices
I Conglomerate/shale, sandstone
II Sandstone and conglomerate
III Green sericitic slates
IV Green sandstone/ violet slates
V Violet sandstones, conglomerates
Kopeh-Dagh basement (Northern Unit)
Marble (Lower Carboniferous)
Limestone, shale, sandstone
(Upper Devonian)
b
Kopeh-Dagh
Turan Plate
Paleotethys suture zone
Iran Plate
a
LAURASIA
Turan Plate
Caspian Sea
Kopeh-Dagh
Paleotethys suture zone
Alborz
Iran Plate
IRAQ
SS Belt
Central Iran
Yazd Block
Tabas Block
Lut Block
Zagros
Neotethys suture zone
EIR
Arabian Plate
Persian Gulf
Makran
Oman Sea
4800
Elevation (m)
0
Tectonic elements
Strike-slip fault
Thrust fault
Syncline
Anticline
Coal horizon
Tunnel (coal mine)
Palynological sample locations
1 Kal-e-Faqir (FQ and MK samples)
2 Kal-e-Bast (KB samples)
3 Kal-e-Jom'eh (MKJ samples)

Figure

Click here to access/download;Figure;Figure_2.jpg

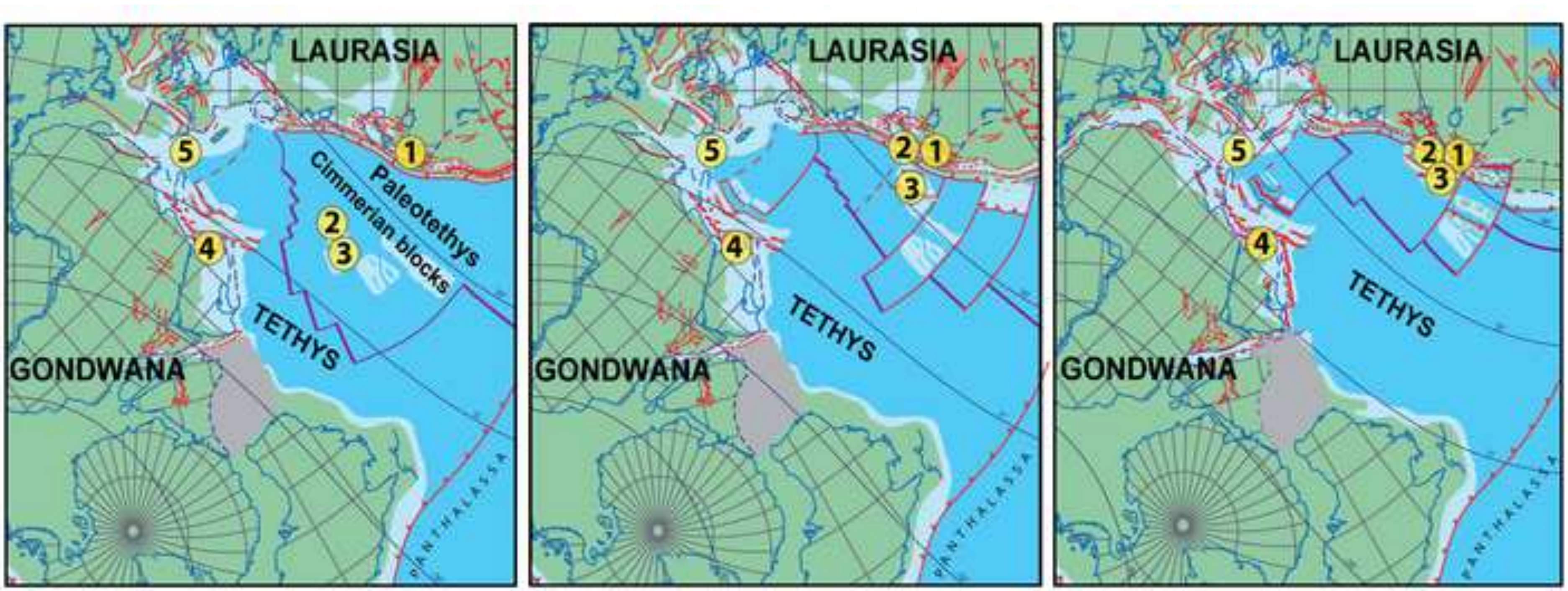

Anisian/Ladinian

Carnian

Norian

Figure

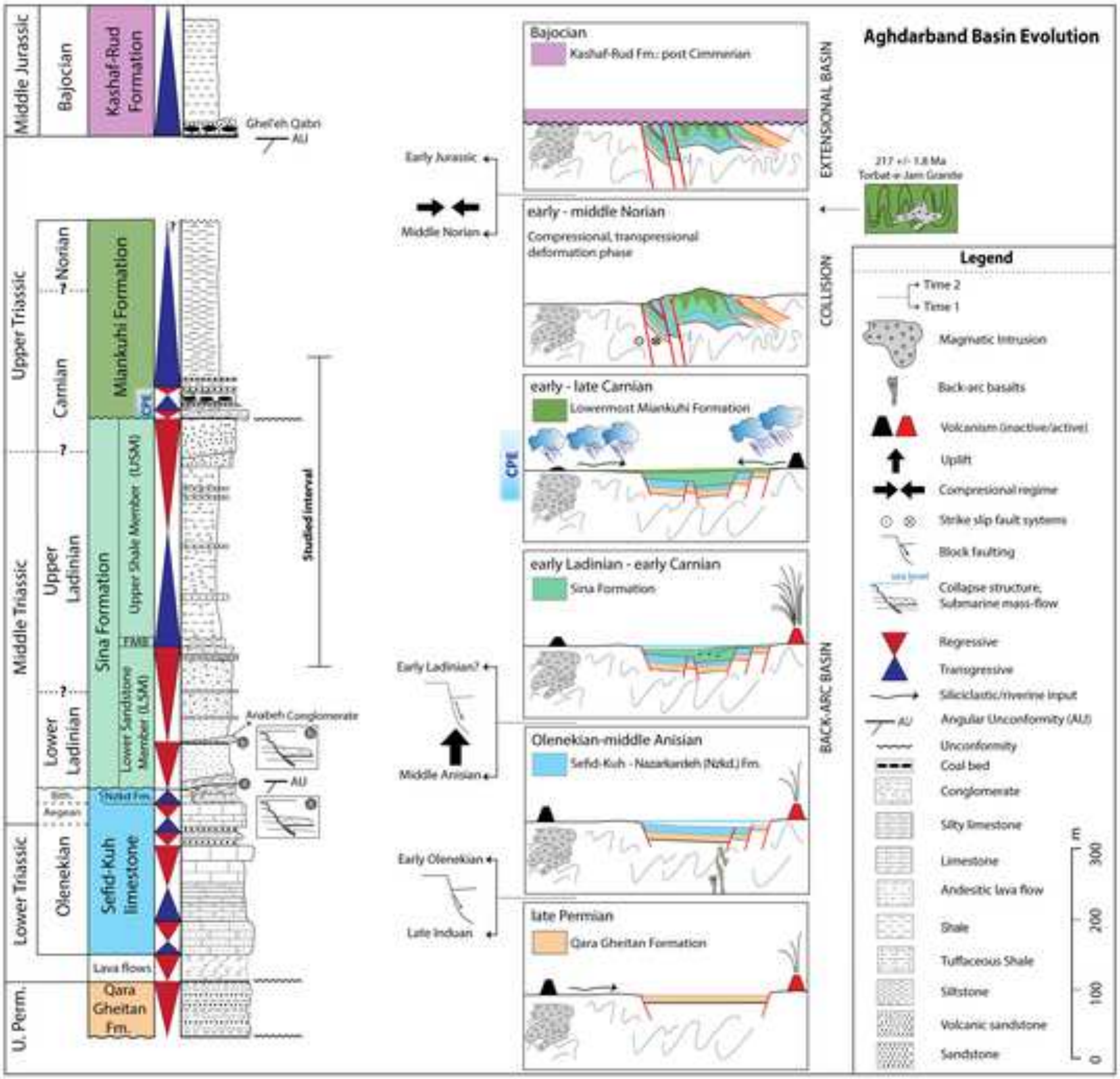

Aghdarband Basin Evolution
Middle Jurassic
Bajocian
Kashaf-Rud Formation
Ghel'eh Qabri
AU
Upper Triassic
Norian
Carnian
Miankuhi Formation
CPE
Middle Triassic
Upper Ladinian
Lower Ladinian
Sina Formation
Upper Shale Member (USM)
Lower Sandstone Member (LSM)
FMB
Studied interval
Anabeh Conglomerate
Lower Triassic
Olenekian
Sefid-Kuh limestone
Nzkd Fm.
Lava flows
U. Perm.
Qara Gheitan Fm.
Early Jurassic
Middle Norian
Early Ladinian?
Middle Anisian
Early Olenekian
Late Induan
Bajocian
Kashaf-Rud Fm.: post Cimmerian
early - middle Norian
Compressional, transpressional deformation phase
early - late Carnian
Lowermost Miankuhi Formation
early Ladinian - early Carnian
Sina Formation
Olenekian-middle Anisian
Sefid-Kuh - Nazarkardeh (Nzkd.) Fm.
late Permian
Qara Gheitan Formation
EXTENSIONAL BASIN
COLLISION
BACK-ARC BASIN
217 +/- 1.8 Ma
Torbat-e Jam Granite
Legend
Time 2
Time 1
Magmatic Intrusion
Back-arc basalts
Volcanism (inactive/active)
Uplift
Compresional regime
Strike slip fault systems
Block faulting
sea level
Collapse structure, Submarine mass-flow
Regressive
Transgressive
Siliciclastic/riverine input
Angular Unconformity (AU)
Unconformity
Coal bed
Conglomerate
Silty limestone
Limestone
Andesitic lava flow
Shale
Tuffaceous Shale
Siltstone
Volcanic sandstone
Sandstone
m
300
200
100
0

Figure

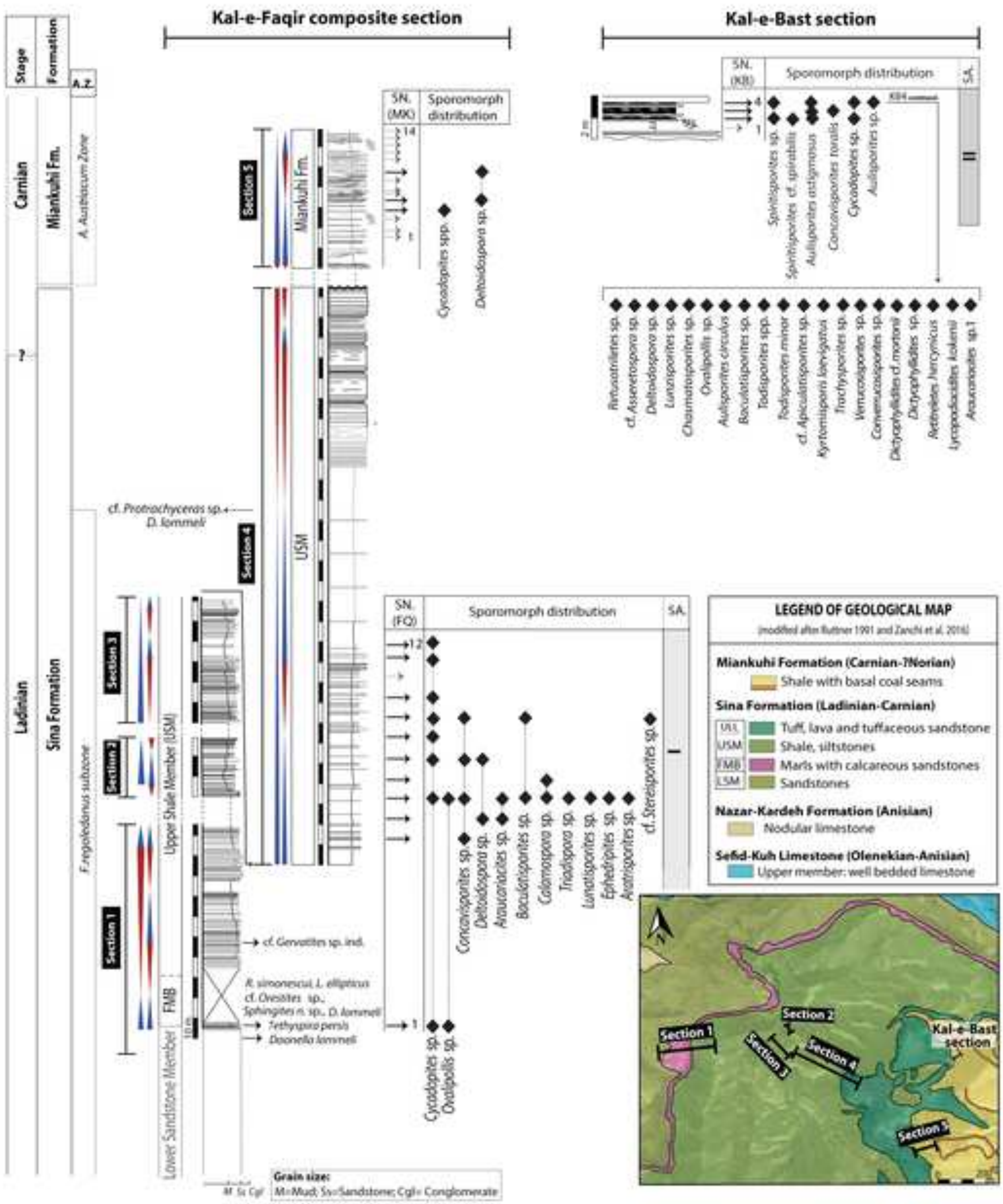
Kal-e-Faqir composite section
Kal-e-Bast section
Stage
Formation
A.Z.
Carnian
Ladinian
Miankuhi Fm.
Sina Formation
A. Austriacum Zone
F. regoledanus subzone
Section 1
Section 2
Section 3
Section 4
Section 5
USM
FMB
Upper Shale Member (USM)
Lower Sandstone Member
SN. (MK)
SN. (FQ)
SN. (KB)
Sporomorph distribution
SA.
cf. Protrachyceras sp.
D. lommeli
cf. Gervatites sp. ind.
Trethyspira persis
Daonella lommeli
Cycadopites spp.
Deltoidospora sp.
Cycadopites sp.
Ovalipollis sp.
Concavisporites sp.
Araucariacites sp.
Baculatisporites sp.
Calamospora sp.
Triadispora sp.
Lunatisporites sp.
Ephedripites sp.
Aratrisporites sp.
cf. Stereisporites sp.
Spiritisporites sp.
Spiritisporites cf. spirabilis
Aulisporites astigmosus
Concavisporites toralis
Aulisporites sp.
Retusotriletes sp.
Ovalipollis sp.
Aulisporites circulus
Baculatisporites sp.
Todisporites spp.
Todisporites minor
Kyrtomisporis laevigatus
Trachysporites sp.
Verrucosisporites sp.
Dictyophyllidites sp.
Araucariacites sp.1
Grain size:
M=Mud; Ss=Sandstone; Cgl= Conglomerate
LEGEND OF GEOLOGICAL MAP
Miankuhi Formation (Carnian-?Norian)
Shale with basal coal seams
Sina Formation (Ladinian-Carnian)
Tuff, lava and tuffaceous sandstone
USM
Shale, siltstones
FMB
Marls with calcareous sandstones
LSM
Sandstones
Nazar-Kardeh Formation (Anisian)
Nodular limestone
Sefid-Kuh Limestone (Olenekian-Anisian)
Upper member: well bedded limestone
Section 1
Section 2
Section 3
Section 4
Section 5
Kal-e-Bast section

Figure

Click here to access/download;Figure;Figure_5.jpg

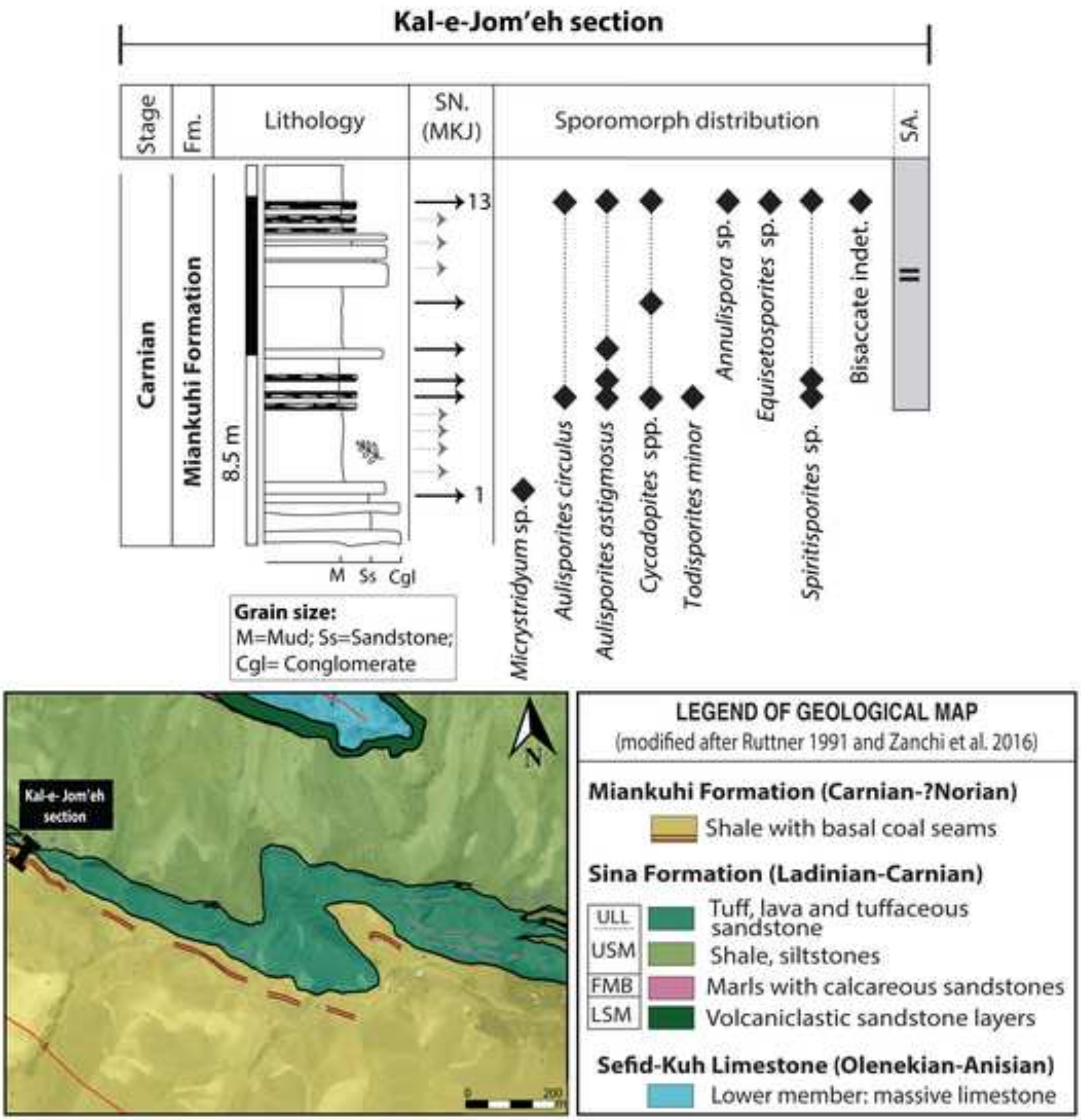

Figure

Click here to access/download;Figure;Figure_6.jpg

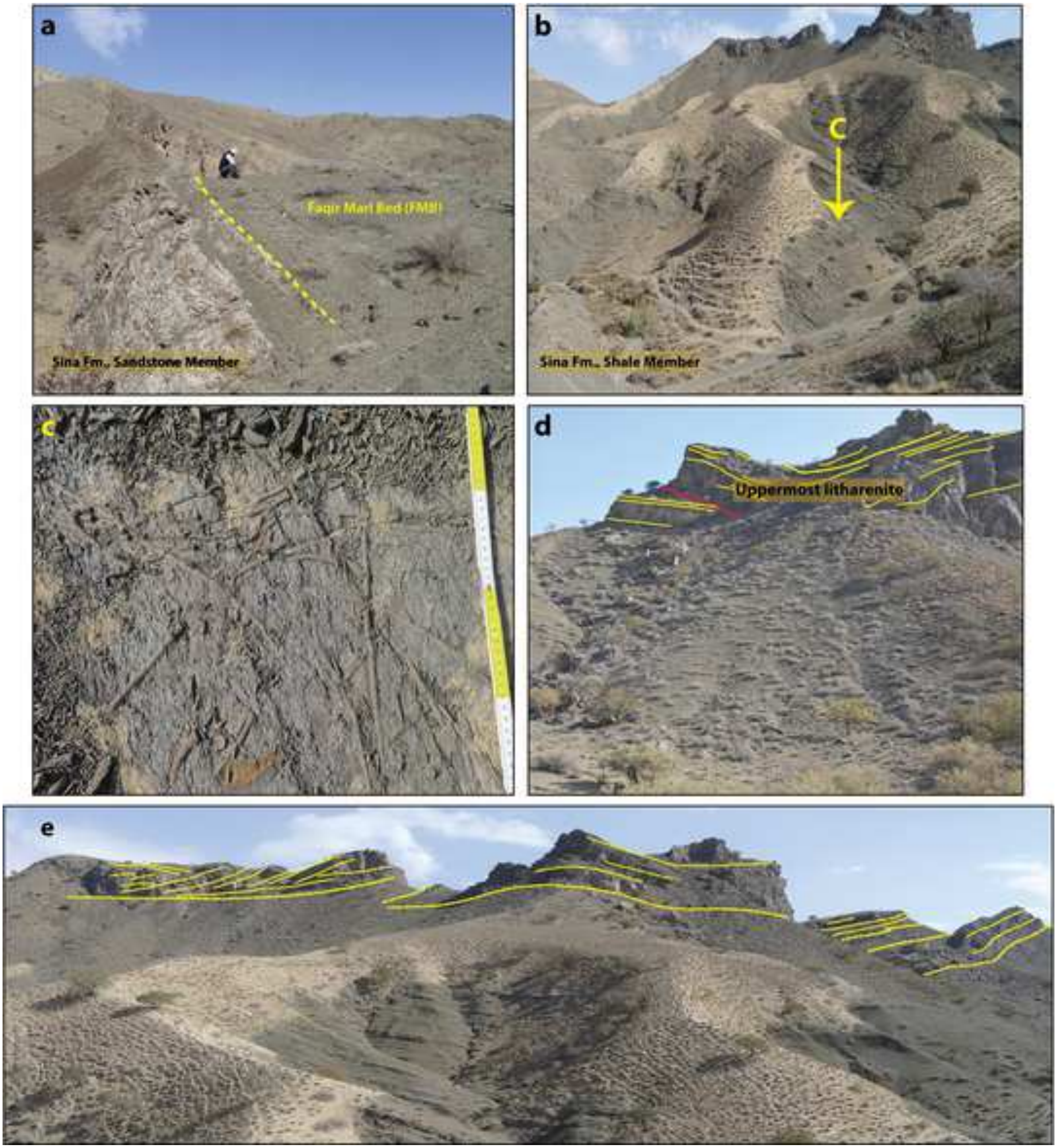

Figure

Click here to access/download;Figure;Figure_7.jpg

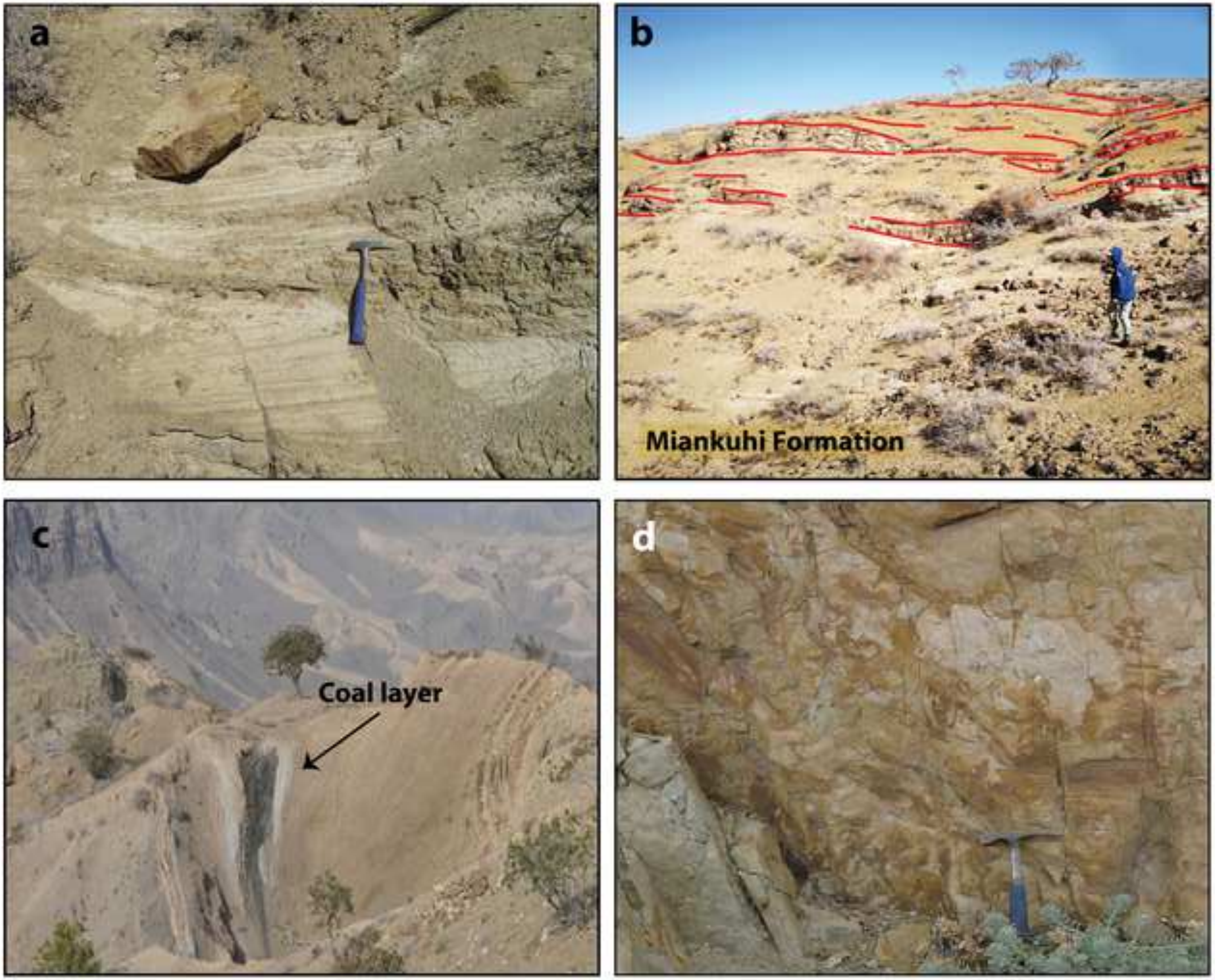

Figure

Click here to access/download;Figure;Figure_8.jpg

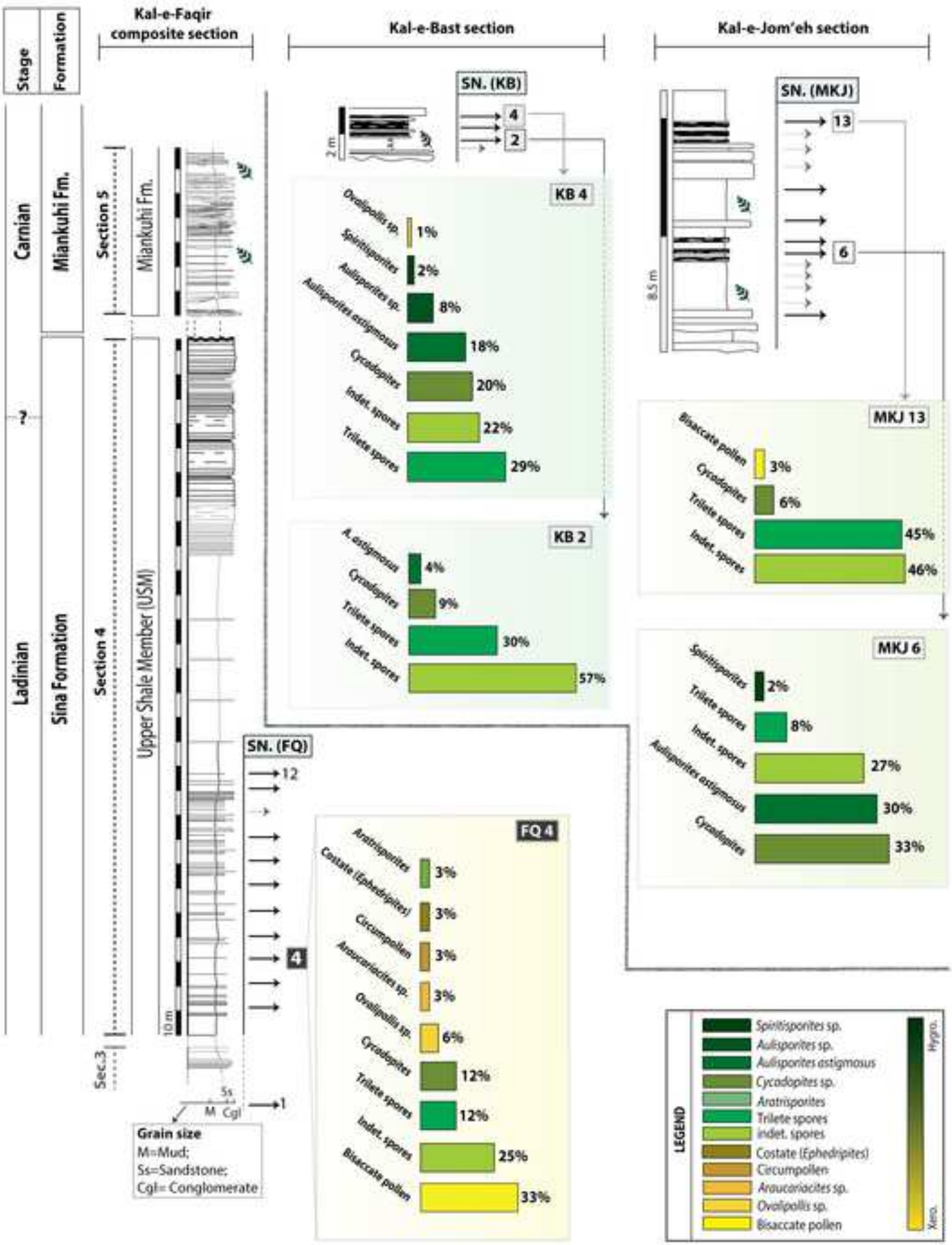

Figure

Click here to access/download;Figure;Figure_9.jpg

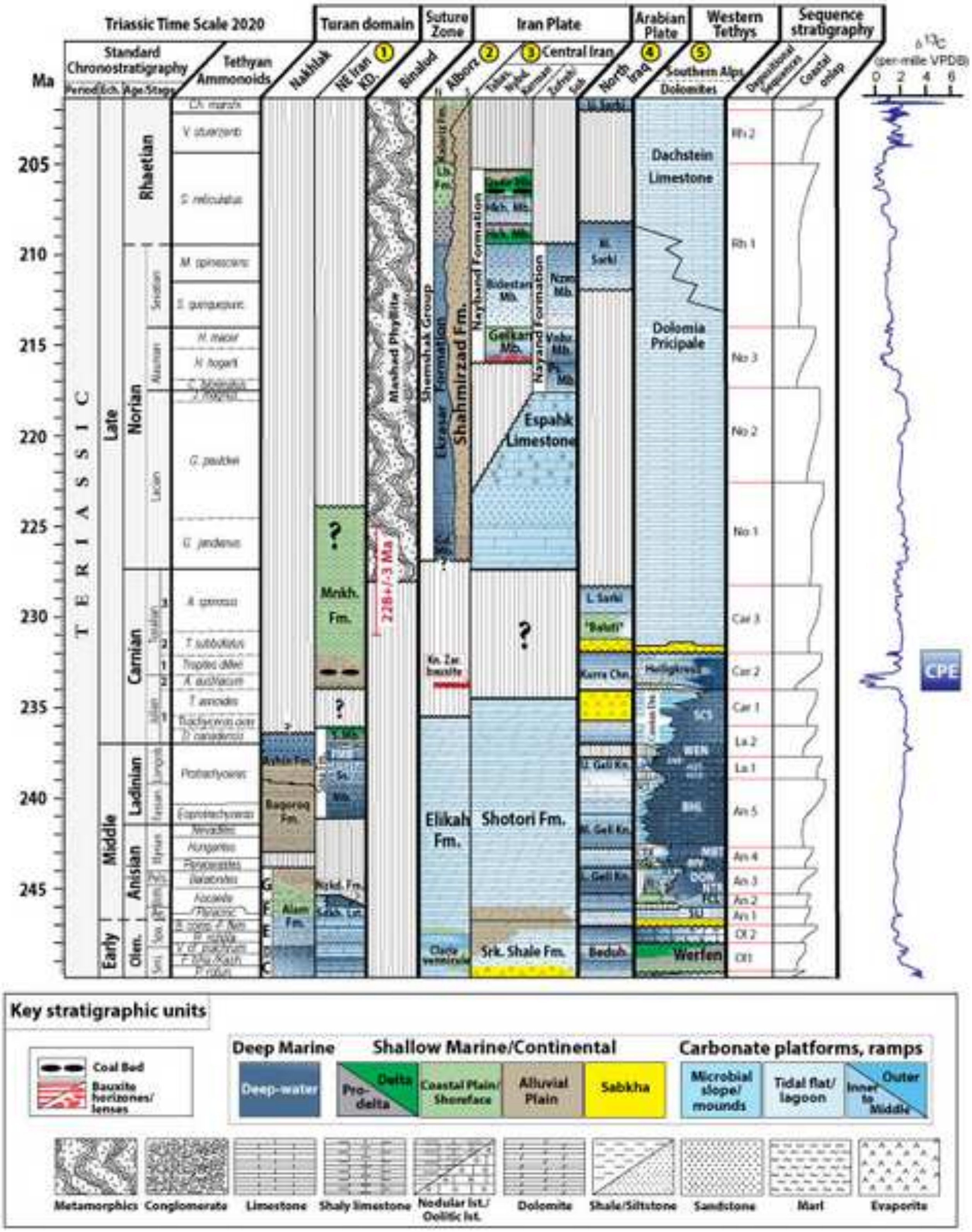

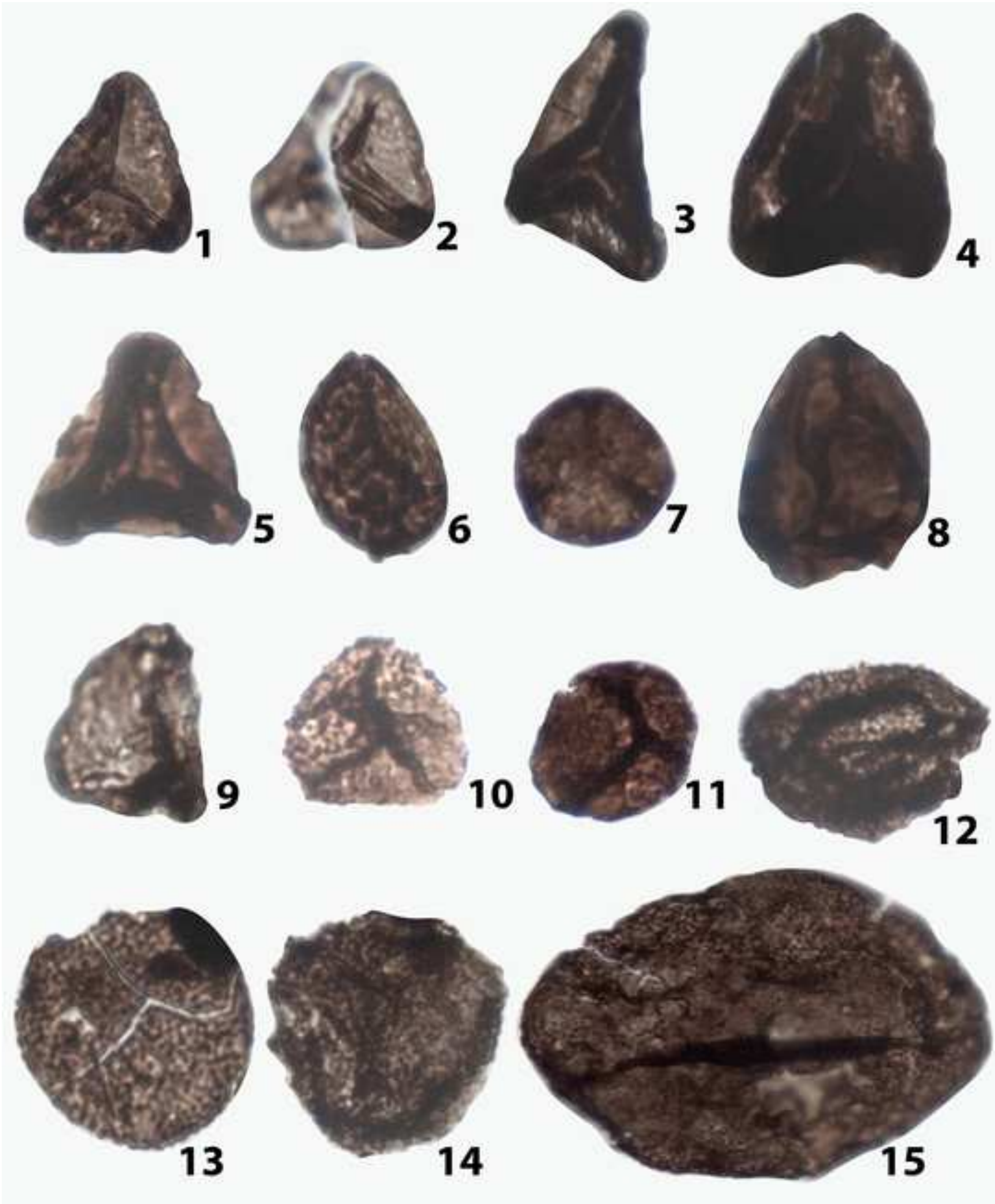
1
2
3
4
5
6
7
8
9
10
11
12
13
14
15

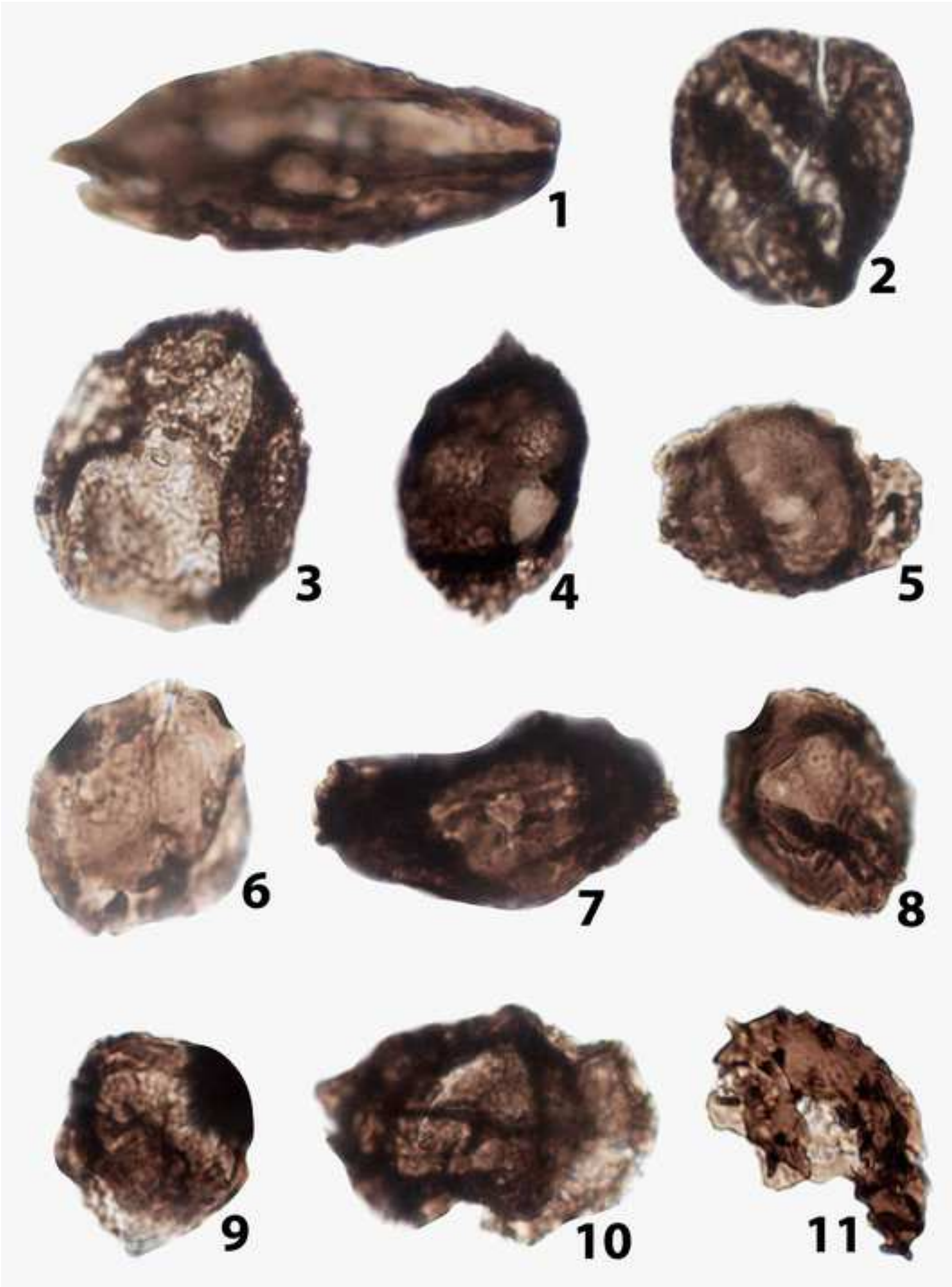


1
2
3
4
5
6
7
8
9
10
11
12
13
14
15

Declaration of interests

☒ The authors declare that they have no known competing financial interests or personal relationships that could have appeared to influence the work reported in this paper.

☐The authors declare the following financial interests/personal relationships which may be considered as potential competing interests: